BEAM SWITCHING REFLECTARRAY WITH RF MEMS TECHNOLOGY

A THESIS SUBMITTED TO
THE GRADUATE SCHOOL OF NATURAL AND APPLIED SCIENCES
OF
MIDDLE EAST TECHNICAL UNIVERSITY

BY

ÖMER BAYRAKTAR

IN PARTIAL FULFILLMENT OF THE REQUIREMENTS
FOR
THE DEGREE OF MASTER OF SCIENCE
IN
ELECTRICAL AND ELECTRONICS ENGINEERING

SEPTEMBER 2007

Approval of the thesis:

BEAM SWITCHING REFLECTARRAY WITH RF MEMS TECHNOLOGY

submitted by **ÖMER BAYRAKTAR** in partial fulfillment of the requirements for the degree of **Master of Science in Electrical and Electronics Engineering Department, Middle East Technical University** by,

Prof. Dr. Canan Özgen _____
Dean, Graduate School of **Natural and Applied Sciences**

Prof. Dr. İsmet Erkmen _____
Head of Department, **Electrical and Electronics Engineering**

Assoc. Prof. Dr. Özlem Aydın Çivi _____
Supervisor, **Electrical and Electronics Engineering Dept., METU**

Prof. Dr. Tayfun Akın _____
Co-Supervisor, **Electrical and Electronics Engineering Dept., METU**

Examining Committee Members:

Prof. Dr. M. Tuncay Birand _____
Electrical and Electronics Engineering Dept., METU

Assoc. Prof. Dr. Özlem Aydın Çivi _____
Electrical and Electronics Engineering Dept., METU

Prof. Dr. Tayfun Akın _____
Electrical and Electronics Engineering Dept., METU

Assoc. Prof. Dr. Şimşek Demir _____
Electrical and Electronics Engineering Dept., METU

Oğuz Şener _____
Manager, ASELSAN

Date: 07.09.2007

I hereby declare that all information in this document has been obtained and presented in accordance with academic rules and ethical conduct. I also declare that, as required by these rules and conduct, I have fully cited and referenced all material and results that are not original to this work.

Name, Last name : Ömer BAYRAKTAR

Signature :

ABSTRACT

BEAM SWITCHING REFLECTARRAY WITH RF MEMS TECHNOLOGY

Bayraktar, Ömer
M. Sc., Department of Electrical and Electronics Engineering
Supervisor: Assoc. Prof. Dr. Özlem Aydın Çivi
Co-Supervisor: Prof. Dr. Tayfun Akın

September 2007, 73 pages

In this thesis 10x10 reconfigurable reflectarray is designed at 26.5 GHz where the change in the progressive phase shift between elements is obtained with RF MEMS switches in the transmission lines of unit elements composed of aperture coupled microstrip patch antenna (ACMPA). The reflectarray is illuminated by a horn antenna, and the reflected beam is designed to switch between broadside and 40° by considering the position of the horn antenna with respect to the reflectarray.

In the design, the transmission line analysis is applied for matching the ACMPA to the free space. The full wave simulation techniques in HFSS are discussed to obtain the phase design curve which is used in determining two sets of transmission line lengths for each element, one for the broadside and the other for switching to the 40°

at 26.5 GHz. The switching between two sets of transmission line lengths is sustained by inserting RF MEMS switches into the transmission lines in each element.

Two types of RF MEMS switches, series and shunt configurations, are designed for the switching purpose in the reflectarray. The phase errors due to nonideal phase design curve and type of the RF MEMS switch are reduced. The possible mutual coupling effects of the bias lines used to actuate the RF MEMS switches are also eliminated by the proper design.

To show the validity of the design procedure, a prototype of 20x20 reflectarray composed of ACMPA elements is designed at 25GHz and produced using Printed Circuit Board (PCB) technology. The measurement results of the prototype reflectarray show that the main beam can be directed to the 40° as desired.

The process flow for the production of the reconfigurable reflectarray is suggested in terms of integration of the wafer bonding step with the in-house standard surface micromachined RF MEMS process.

Keywords: Reflectarray, RF MEMS, Reconfigurable antennas, Micromachining, Wafer bonding.

ÖZ

RF MEMS TEKNOLOJİSİ İLE AYARLANABİLİR YANSITICI DİZİ ANTENİ TASARIMI

Bayraktar, Ömer
Yüksek Lisans, Elektrik ve Elektronik Mühendisliği Bölümü
Tez Yöneticisi: Doç. Dr. Özlem Aydın Çivi
Ortak Tez Yöneticisi: Prof. Dr. Tayfun Akın

Eylül 2007, 73 sayfa

Bu tezde, yarık bağlaşımlı mikroşerit yama anteninden oluşan, hüzme yönü RF MEMS anahtarlar yardımı ile ayarlanabilen yansıtıcı dizi anteni tasarımı sunulmaktadır. Ayarlanabilir dizi anteni 26.5 GHz de tasarlanmış olup 10x10 dizi elemanından oluşmaktadır. Yansıtıcı dizi anteni, ana hüzmenin yönü dizi anteni düzlemine dik yönde ve 40 derece arasında RF MEMS anahtarlar yardımı ile değiştirilebilecek şekilde tasarlanmıştır. Tasarımda besleme olarak kullanılan huni anteninin dizi antenine göre pozisyonu da hesaba katılmıştır.

Tasarımda yarık bağlaşımlı mikroşerit yama antenini için geliştirilmiş olan iletim hattı modeli, antenin uzaya uyumlanmasında kullanılmıştır. Faz tasarım grafiğini elde etmek amacı ile HFSS de elektromanyetik benzetim teknikleri incelenip uygun

olan yöntem ile grafik elde edilmiştir. Faz tasarım grafiği yardımı ile yansıtıcı dizi içerisindeki yarık bağlaşımlı mikroşerit yama antenlerinin iletim hattı uzunlukları iki küme şeklinde belirlenmiştir. Birinci kümedeki uzunluklar hüzmenin 26.5GHz de dizi antenine dik olan yöne yönelmesini, ikinci kümedeki uzunluklar ise hüzmenin 26.5GHz de 40 dereceye yönelmesini sağlamaktadır. İletim hatlarının uzunluk değerlerinin birinci küme ile ikinci küme arasıda değiştirilmesi, iletim hatlarının üzerine yerleştirilen RF MEMS anahtarlar yardımı ile sağlanmaktadır.

İletim hatlarında anahtarlamayı sağlamak amacı ile seri ve paralel olmak üzere iki çeşit RF MEMS anahtar yapısı tasarlanmıştır. İdeal olmayan faz grafiğinden ve RF MEMS anahtar çeşidinden kaynaklanan hatalar azaltılmıştır. RF MEMS anahtarlarının elektriksel uyarımını sağlayan besleme hatlarından kaynaklanabilecek olası karşılıklı bağlaşım hataları, hatların uygun tasarımı ile önlenmiştir.

Tasarım yönteminin geçerliğini gösermek amacı ile yarık bağlaşımlı mikroşerit yama antenlerinden oluşan 20x20 prototip yansıtıcı dizi anteni, 25GHz de tasarlanıp baskı devre yöntemi ile üretilmiştir. Prototip yansıtıcı dizi anteninin ölçüm sonuçları ana hüzmenin istenildiği gibi 40 dereceye döndürülebileceğini göstermiştir.

Ortadoğu Teknik Üniversitesi Mikroelektronik Tesislerinde (ODTÜ-MET) geliştirilen ve yüzey işleme tekniğine dayanan, mikroişleme üretim sürecinin yansıtıcı dizi anteni üretimine uyarlanması amacı ile pul bağlama aşamasının bu sürece nasıl ekleneceği tartışılmış ve uygun bir öneri sunulmuştur.

Anahtar Kelimeler: Yansıtıcı dizi anteni, RF MEMS, Ayarlanabilir antenler, Mikroişleme, Pul bağlama.

To My Family

ACKNOWLEDGEMENTS

I would like to express my acknowledgements to everyone who helped in completing this thesis. First of all, I would like to thank my advisors Assoc. Prof. Dr. Özlem Aydın Çivi and Prof. Dr. Tayfun Akın for their invaluable supervision, encouragement, patience and guidance to reach my goals during my research. I am also thankful to Assoc. Prof. Dr. Şimşek Demir for his great effort while solving my problems as well as his friendly attitude in his supervision at my undergraduate years. I also would like to thank to Prof. Dr. Altunkan Hızal for sharing his experience, suggesting useful materials to study and supplying us Millimeter and Microwave laboratories.

I also would like to thank Dr. Kağan Topallı and Mehmet Ünlü not only for their contributions to my thesis by sharing their invaluable experiences, but also for being my elder brothers who I can consult about anything in my life. I also would like to thank them for their teachings during the laboratory lectures.

I would like to express my appreciation to Engin Ufuk Temoçin for his great and invaluable willingness to help and encourage me in completing my thesis. I would like to thank Ömer Özgür Yıldırım for reflecting his optimistic sight of life on our friendship. My special thanks also must go to İpek İstanbulluoğlu for her sincere and friendly attitude that I will never forget, and I would like to thank for every help and support she made. I also would like to thank my colleague Halil İbrahim Atasoy for his friendship during two year of my undergraduate study. I would like to express my special gratitudes to Yusuf Bahadır Turhan for his encouragement and moral support that made me very happy. I also would like to thank to whole MEMS-VLSI group for their friendship. I would like to thank METU-MET personal for their support during the RF MEMS device fabrications.

I am also grateful to my home mates, Hasan Örten, Ömer Akşen, and Adnan Kalay, for being excellent friends and for their great help during both my undergraduate and graduate studies.

Last but certainly not least, my heartfelt thanks go to my father İlhan Bayraktar and my mother Neriman Bayraktar, as well as my sister, Emel Burkut, for their genuine support, love, understanding, and constant encouragement. Without them this work would had never been completed.

This work is partially supported by the Scientific and Technical Research Council of Turkey (TÜBİTAK), State Planning Organization of Turkey and Advanced MEMS for RF and Millimeter Wave Communication (AMICOM).

TABLE OF CONTENTS

LIST OF TABLES

LIST OF FIGURES

CHAPTER I

INTRODUCTION

In recent years, reflectarray applications attract the scientist's attention due to their advantages over the reflector antennas and phased array antenna systems. The reflectarrays will certainly become more attractive when reshaping the beam of the reflectarray by electrical excitement is succeeded. The main goal of this thesis is to design a reconfigurable reflectarray where the beam is switched between two angles by electrical actuation of Radio-Frequency Micro-Electro-Mechanical-System (RF MEMS) switches inserted into the elements of the reflectarray.

In this chapter, Section 1.1 gives the overview of the reflectarray in terms of the definition and types of the reflectarrays. Section 1.2 explains the detailed objectives and organization of the thesis.

1.1. REFLECTARRAY OVERVIEW

1.1.1. Definition and Historical Improvement of the Reflectarray

The reflector antennas utilize the geometrical optics to shape the beam while the amplitude and phase of the excitation of each element in the phased array antennas are properly adjusted to obtain desired radiation pattern. The reflector type antennas are advantageous in the sense that they eliminates the complex feed system in the phased array antennas but they produce a unique radiation pattern for a given feed

position and the reflector shape and the radiation pattern of the reflector antenna can be scanned only by mechanical rotation. On the other hand, the radiation pattern of the phased array antenna can be varied without changing the geometry of the antenna and beam is scanned electronically. In 1963, Berry et al. introduced the idea of combining the features of the reflector and array type antennas [1]. They constructed the first reflecting surface composed of arrays of elementary antennas called reflectarray. In the reflectarray antenna, conventional array theory [2] is used to obtain various beam shapes using the same aperture without the need for a complex feeding system. The idea depends on proper adjustment of the reflection phase values from each element to form a desired equiphase plane as shown in Figure 1.1. The phase shifting geometry in the reflectarray is not a complex and separate system but it is usually a part of the antenna dimension. Berry et al. [1] used waveguide with shorted back as an elementary antenna in the reflectarray structure. The required phase shift for each element is achieved by the position of the short circuit in the waveguide.

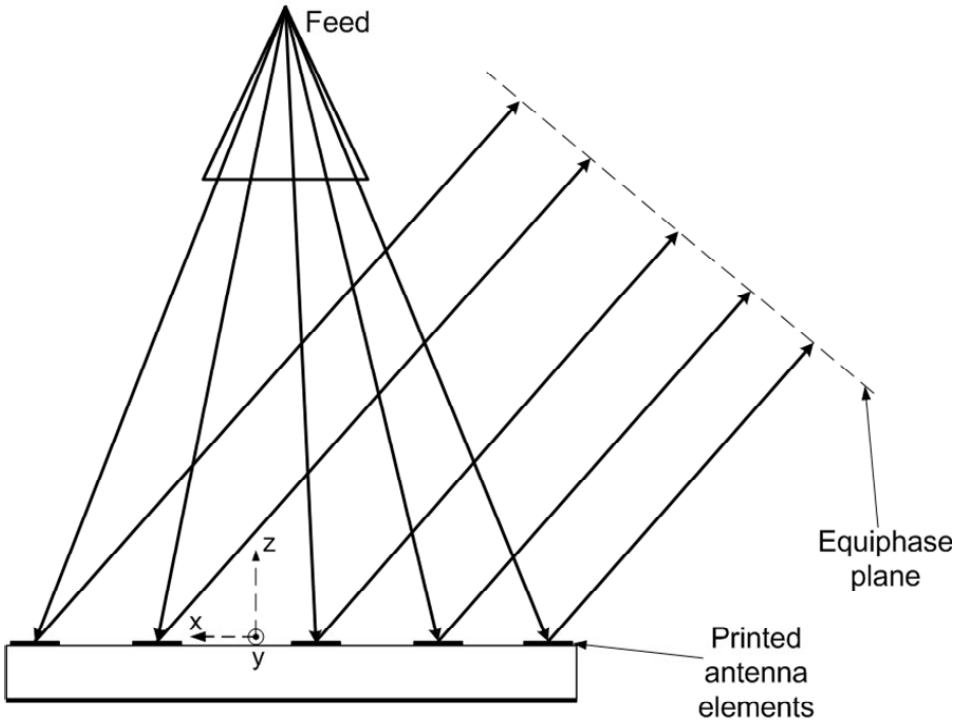

Figure 1.1: The reflectarray structure.

The reflectarray technology has gone into a great development in terms of both the type of the elementary antenna and the analysis methods in last 30 years. The bulky structure of the waveguide is eliminated by the suggestion of the microstrip reflectarray by Malagisi in 1978 [3]. Today, the microstrip reflectarrays have many advantages compared to the parabolic reflectors and electronically scanned phased array antennas. In addition to the feeding through the free space to eliminate the losses of a microstrip feed network limiting the performance of high-gain millimeter wave arrays [4], microstrip reflectarray has less mechanical complexity and can be conformed to any given surface. Furthermore, the microstrip reflectarrays have small size, low weight and low cost.

The beam reconfigurability can be obtained by adding an electrical relay to the phase shifter structure of the elementary antenna such that the phase of the reflected field can be adjusted by electrical actuation. There are different reconfigurable phase shifter models that can be used for this aim. The electrical relay in the reconfigurable phase shifters can be constructed using ferrite material, positive intrinsic negative (PIN) diodes, Field Effect Transistor (FET) switches or RF MEMS switches. The ferrite phase shifters provide high isolation and low switching time but they have high cost and weight. PIN diodes have small sizes compared to the ferrite phase shifters and they have higher isolation compared to the FET switches but they dissipate high power due to their need for continuous bias current. RF MEMS switches provide low loss characteristics compared to the PIN diodes and FET switches. They have very low power consumption. Since they can be constructed on many substrates like glass, silicon, ceramic, they can be built on the same substrate connected monolithically to other components such as microstrip patch antenna. RF MEMS switches seem to be the best candidate for the construction of reconfigurable reflectarray in terms of its low cost and high electrical performance. However, the RF MEMS switches have not fully taken its place in the commercial area due to reliability and packaging problems.

Today there are many space applications of the reflectarrays [5] such as Direct Broadcast Satellite (DSB) application [6] for the coverage of Europe and DSB with multibeam functionality [7] for the coverage of both South America and the Florida regions. Local Multipoint Distribution System (LMDS) application presented in [8] can be used in the mobile communications, internet access and video. Three different reflectarrays have recently been developed for National Aeronautics and Space Administration's (NASA) future deep-space and Earth remote sensing missions and NASA/Jet Propulsion Laboratory's (NASA/JPL) Wide Swath Ocean Altimeter (WSOA) radar application [9]. The reflectarrays are also used in the automotive radar applications where long range and narrow beam are required [10].

1.1.2. Types of reflectarrays

The reflectarrays can be classified as passive reflectarrays, active reflectarrays, contoured beam and multi-beam reflectarrays, and reconfigurable reflectarrays. However, this classification is not so distinct and some of the reflectarrays can be examined in more than one class [7].

1.1.2.1. Passive Reflectarrays

The passive reflectarrays do not contain active devices. There are different phase shifting mechanisms introduced in literature for the passive reflectarrays. The variable stub loaded patch antenna is used as a phase shifting device such that the reflection phase is the twice of the length of the open circuited stub connected to the edge of the patch antenna [11]. The spurious radiation due to the open circuited stub is eliminated in the reflectarray element of microstrip patches with variable resonant length [12] or variable length crossed dipoles [13]. These structures offer lower loss and cross polarization compared to the stub loaded patch antenna but the bandwidth is limited by the patch or dipole size. The bandwidth of the variable size patch

reflectarray is increased by stacking two [14] (or three [15]) patch antennas on top of each other with the dielectric layer between them and phase shift is sustained by changing the dimension of the patch antenna closest to the ground plane.

If the circularly polarized antenna element is rotated, the phase of the radiated field is also delayed or advanced (depending upon the direction of rotation) by the same amount of the rotation angle. This feature is used to build a circularly polarized reflectarray [16] with reduced cross polarization level compared to the stub loaded patch antenna elements.

Aperture coupled microstrip patch antennas are used as a reflectarray element for single or dual polarization [17]. It is also possible to use this structure for the circular polarization. In this configuration the reflection phase is determined from the length of the open circuited transmission line at the feed substrate coupled to the patch antenna on top of the antenna substrate through the aperture on the ground plane between two substrates. In [18], the large range of phase delay which improves the bandwidth [19] is obtained by increasing the one side of the U-shaped transmission line and using the other side as a matching stub.

1.1.2.2. Active Reflectarrays

The use of Metal Semiconductor Field Effect Transistor (MESFET) amplifier in dual polarized aperture coupled microstrip patch reflectarrays is shown in [20]. The active circuit network constructed at the transmission line of the dual polarized aperture coupled microstrip patch antenna (ACMPA) sustains the amplification of the reflected signal with a proper phase shift determined from the reflection direction. However, the active reflectarrays has no significant advantage over the phased arrays due to the high power consumption of the FET amplifiers and the high production cost of the large arrays.

1.1.2.3. Contoured Beam and Multi-Beam Reflectarrays

Contoured beam reflectarrays are designed to cover a predefined region and they differ from the pencil beam reflectarrays in covering larger areas. The design is made by adjusting the required phase values determined from the distance between the predefined coverage area and the reflectarray elements. The application of the contoured beam reflectarray using microstrip patches of variable size shown in [6] is designed for Direct Broadcast Satellite (DSB) application for the coverage of Europe. This design has achieved 23dB gain in the 99% coverage but it suffers from the low bandwidth (7%) and reduced aperture efficiency. The bandwidth can be improved by using parabolic surface to print patch antennas [21] which disturbs the reflectarray advantage of being flat. It is offered in [6] that the antenna parameters can be improved in the frequency band by applying optimization on the phase distribution which is found by a direct phase synthesis method at the resonant frequency.

In the reflectarrays the amplitude of the reflected field at the unit element is determined by the radiation of the feed antenna at that point. Hence, the phase-only synthesis method is used to determine the phase distribution of the elements. The phase only-synthesis method based on "Intersection Approach [22]" is used for the countered beam reflectarray with large number of elements [23] and the measurement results [7] of the produced contoured beam indicates 10% bandwidth which is acceptable for DSB applications. The other application of the contoured beam reflectarray that meets the specification for Local Multipoint Distribution System (LMDS) is presented in [8].

The reflectarrays can be designed to produce multi-beam using single or multiple feeds. The contoured beam reflectarray designed for the DSB application in [7] has also a multibeam functionality for the coverage of South America and the Florida

regions with one feed. The example for multibeam reflectarray using multiple feeds is presented in [24] designed for LMDS applications.

1.1.2.4. Reconfigurable Reflectarrays

The radiation pattern of the reflectarray can be changed or rotated by using reconfigurable materials or switches in the phase shifter part of the unit element such as tunable dielectrics, varactor diodes, PIN diodes, MEMS structures (micro-motors, etc.) or RF MEMS switches.

It is possible to construct a reconfigurable reflectarray consisting of patch elements on tunable dielectric such as ferroelectric films and Liquid Crystals (LC). The phase shifter structure composed of series coupled microstrip lines connected to open circuited radial stubs are printed on a ferroelectric thin film of $Ba_{0.6}Sr_{0.4}TiO_3$ in [25]. The phase shifter is wire bonded to the patch antenna and phase swing is achieved by applying bias voltage to the dielectric. The measured 5 dB insertion loss and high bias voltage up to 350 V are disadvantages of the structure. By using the nematic LC the maximum control voltage of 15 V can be obtained [26]. The applications of nematic LC for reflectarrays are shown by two examples in [27]. The first example is filling the cavity under the patch antenna with LC and changing the permittivity of LC by electrical bias to sweep the frequency. In the second example, the cavity under the transmission line in the aperture coupled patch antenna configuration is filled with LC. In both cases, thin cavities are used under the metal region and hence the thickness of LC is reduced to obtain fast alignment of the LC molecules increasing the switching time. In the aperture coupled patch configuration, larger phase range can be swept by increasing the transmission line length and multiple of 360° phase swing can be obtained. The measurement results for both configurations [26] showed that the 270° phase swing with a maximum reflection loss of 8 dB is obtained for the patch configuration while the aperture coupled configuration showed the phase

swing of 240° with maximum reflection loss of 15 dB. The worse results for the aperture coupled configuration arise from the production inaccuracy at 35 GHz such that it is difficult to make a correct alignment of the small aperture.

The varactor diodes can be implemented between the radiating edge of the patch antenna and the ground plane such that the radiating susceptance of the patch antenna is varied by the capacitive loading introduced by the varactor diode [28]. This configuration introduces a phase swing of 180° which is the case for a pure capacitive loading. In the design proposed in [29] two identical patch antennas with a small gap between them are connected together with the varactor diodes. The antennas in the reflectarray are connected to an array of digital to analog converters to determine the voltage drop at the varactor diodes. By proper adjustment of the patch dimension and the voltage drop at the diodes the phase swing of 360° is obtained but it suffers from a narrow bandwidth. The 8% percent bandwidth is obtained in the configuration shown in [30] that uses periodic varactor diodes on a surface. The reflection phase is adjusted by changing the sheet capacitance and inductance as a result of the proper adjustment of the diode voltages. The surface behaves as an artificially constructed magnetic conductor that can steer the beam $\pm 40°$ in two dimensions for both circular and linear polarizations.

There are some examples of the reconfigurable reflectarrays that employs the MEMS structures and diodes. The mechanically rotatable patch antennas are proposed in [31] without the production of the structure where the rotation of the patch antennas are provided by micro machined motors under each patch antenna. The other concept is given by Raytheon Company for the circular polarization in the patented work describing the production method with no measurement results. The idea depends on rotating the dipole antenna with the help of diodes [32] or MEMS switches [33]. The structure consists of circular patch at the periphery of which the series of stubs are arranged such that two opposing stubs are connected to the circular patch with the help of diode or MEMS switches while the others are disconnected. The same phase

shifting structure is presented by Alcatel [34] but reflectarray structure is not formed. The simulation technique using finite difference time domain (FDTD) algorithm for the phase shifter structure proposed by Alcatel is given in [35]. The examples of phase shifter structure for the steerable reflectarray using electrically and optically actuated MEMS switches used to adjust the length of the dipole antenna are given in [36] and [37] without the production and measurement of the whole reflectarray. There are also a plenty of reconfigurable phase shifters with RF MEMS switches developed at different frequencies [38] and they can be directly connected to aperture coupled microstrip patch elements. The reconfigurable planar phase shifter surface consists of three patch sections with a gap of 0.5 mm between them is developed in [39] without constructing the whole reflectarray. There are two gaps on each of which 5 RF MEMS switches are implemented resulting a total number of 10 RF MEMS switches. Hence the phase swing of 360° is tried to be covered by 2^{10}=1024 phase states and maximum phase shift of 10° between two successive states is obtained. Furthermore, the phase scaling technique is adopted for this configuration where the phase shift is calculated by the interpreting the phase shifter as a cascaded scale change networks and the sensitivity regarding the losses due to RF MEMS switches is also discussed in [40].

Other than the reflectarray designed in this thesis, there are two other reconfigurable reflectarrays developed within the European Network of Excellence of Advanced MEMS for RF and Millimeter Wave Communication (AMICOM). The first configuration given in [41] is designed at 26GHz with RF MEMS switches and a prototype is produced. Reflectarray operating at 26GHz consists of aperture coupled microstrip patch antennas where the coplanar waveguide couples to the patch antenna through the aperture on ground plane. 7 state phase shifter is constructed using short circuited coplanar waveguide loaded by 6 MEMS switches. A prototype array composed of 10x10 elements with 600 RF MEMS switches is fabricated on Silicon. The beam is switched between four angles of 90°, 105°, 120° and 135° in the elevation plane. The second reconfigurable reflectarray is developed by Perugia [42]

within the AMICOM. The reflectarray consists of aperture coupled microstrip patch antennas where the microstrip transmission lines are coupled to the patch antennas through the aperture on ground plane. The transmission lines are loaded by open ended microstrip stubs with MEMS capacitances in order to obtain the phase shifting capability. A prototype of 20x20 element reflectarray with fixed length transmission lines without the RF MEMS switches to rotate the beam to 45 degrees is fabricated and measured. The measurement results show that the beam of the antenna is rotated to required direction.

1.2. THESIS OBJECTIVES AND ORGANISATION

The main goal of this thesis is to design a reconfigurable reflectarray where the beam switching is sustained by the RF MEMS switches. The reflectarray consists of aperture coupled microstrip patch antennas. The transmission line length of each element is changed by RF MEMS switches to provide required phase shift to rotate the beam. The specific objectives are summarized as follows:

- The analysis of the aperture coupled microstrip patch antenna (ACMPA) with its equivalent transmission line model as an initial design stage of obtaining the matching.
- Obtaining the phase characteristics with respect to the length of transmission line in the ACMPA configuration for the design of the reflectarray.
- Improving the phase characteristics to reduce the errors due to non idealities in the characteristics.
- Designing possible RF MEMS switch types that can be integrated to the ACMPA for the phase switching purpose.
- Reducing the mutual couplings that arise from the RF MEMS switch type and bias lines.
- Verifying the reflectarray concept by the designing a prototype.

- Introducing the process flow that can be followed in the production of the reconfigurable reflectarray.

After this introduction chapter the thesis is organized as follows:

Chapter II gives brief information about ACMPA and describes its transmission line analysis. The analysis steps are given to obtain the matching of ACMPA to the free space.

Chapter III introduces how to obtain phase design curve with full wave simulations in HFSS for the general reflectarray design and in particular the reconfigurable reflectarray is designed by describing the attempts to reduce the adverse effects of nonideal phase design curve and RF MEMS switches in the phase shifter part.

Chapter IV presents a process flow that describes the integration of the wafer bonding step with the surface micromachining based process that have already been developed at the Middle East Technical University Microelectronic Facilities (METU-MET) for the production of various RF MEMS switches.

Chapter V concludes the work carried out through this research with possible suggestions of the future improvements.

CHAPTER II

APERTURE COUPLED MICROSTRIP PATCH ANTENNA

This chapter introduces the aperture coupled microstrip patch antenna (ACMPA) used as an element in the design of the reconfigurable reflectarray in this thesis. Section 2.1 presents the operating principles and properties of ACMPA. Then, Section 2.2 describes the transmission line equivalent circuit of ACMPA to obtain matching of single ACMPA to the free space.

2.1. OPERATING PRINCIPLE AND PROPERTIES OF ACMPA

The general structure of aperture coupled microstrip patch antenna is shown in Figure 2.1. In this thesis, a reconfigurable reflectarray is designed so that the phase of the scattered field will be controlled by inserting variable length microstrip transmission line coupled to the patch by means of an aperture in the ground plane. For the reflectarray application, the excitation point at the transmission line shown in Figure 2.1 is left as an open circuit and the length of the microstrip transmission line is changed by ON and OFF positions of the RF MEMS switches. The patch antenna is printed on an antenna substrate which is bonded to feed substrate on which microstrip line with RF MEMS switches are implemented. The ground plane between the antenna and feed substrate prevents the interference effects on the scattered field due to tuning elements. By the low loss and high isolation

characteristics of the MEMS switches, it is also possible to prevent the amplitude and phase nonuniformities and so that the array characteristics are not affected.

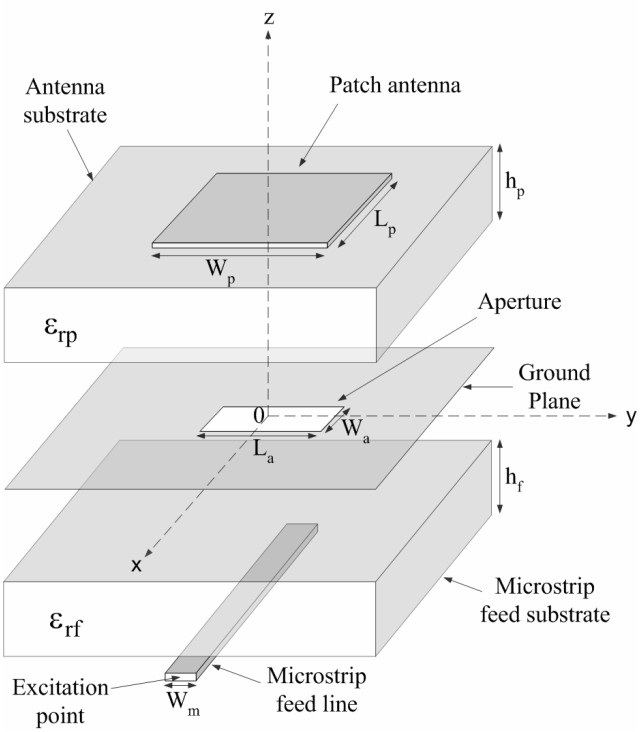

(a)

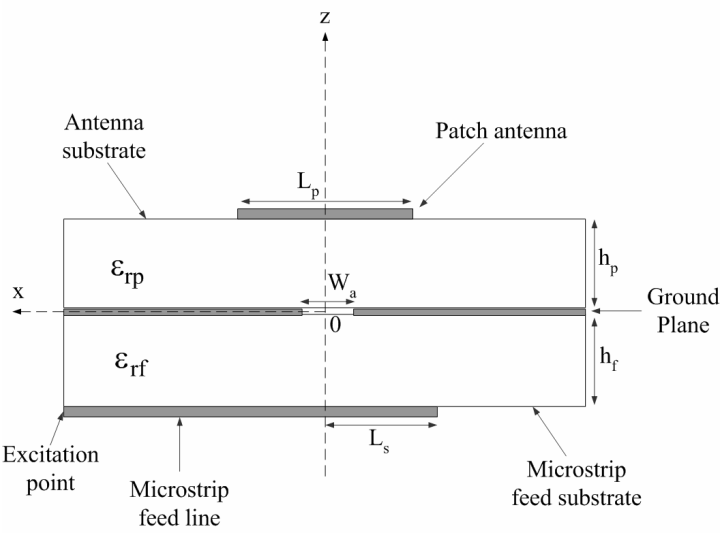

(b)

Figure 2.1: (a) Expanded and (b) side view of an aperture coupled microstrip patch antenna.

The principle of operation of the reconfigurable reflectarray composed of ACMPA elements is as follows. The patch antenna printed on the antenna substrate receives the electromagnetic wave linearly polarized in the x-direction. Then, the electromagnetic wave couples to the microstrip line printed on a feed substrate by means of an aperture on the ground plane between two substrates. Since the microstrip transmission lines are open ended, the wave fully reflects back and couples to the patch antenna using the aperture on the ground plane. The distance that the wave propagates on the transmission line determines the phase of the reflected field. The RF MEMS switches implemented on the microstrip line are used to change the length of the line, that is, the phase of the reflected field is changed by using RF MEMS switches. Hence, the phase of the reflected field from each unit element of the reflectarray can be changed by determining the location of the RF MEMS switches so that the main beam can be rotated to the desired direction.

This configuration has many advantages. First of all, a separate substrate is used for the transmission line and there is more space for extending the line length to obtain large phase delay. Second, the large space at the feed substrate can be used to insert active elements and RF MEMS switches for reconfigurable reflectarrays [43]. Third, the use of two separate substrates introduces the flexibility of choosing the high dielectric substrate for the phase shifters if required while the microstrip patch antenna must be printed on a low dielectric substrate in order to increase the bandwidth, radiation efficiency and the steering range without scan blindness [44]. Fourth, the feeding through aperture is simple to construct compared to the probe feed microstrip antenna and the large self reactance of the probe is also eliminated [45]. Finally, the spurious radiation due to the transmission line is backwards and does not disturb the radiation pattern of the patch antenna due to the ground plane between them. Moreover, the spurious radiation and hence the power loss can be eliminated by inserting a ground plane on top of the transmission lines.

There are three different methods that can be used in the analysis of the ACMPA which are transmission line method [46], cavity method [47] and full wave electromagnetic models such as integral equation/moment method (MoM) [48], finite element method (FEM) or finite difference time domain method (FDTD) [49]. In this study, the transmission line analysis method is used in the initial determination of the dimensions of ACMPA for obtaining the matching to the free space and it is discussed in Section 2.2 in detail. Then the full wave electromagnetic (EM) simulation tool High Frequency Structure Simulator (HFSS) based on the numerical solution technique of FEM is used for fine tuning of the antenna. Finally, the reflectarray structure is simulated in HFSS to obtain the phase design curve showing the reflection phase values versus transmission line length.

2.2. TRANSMISSION LINE MODEL

The transmission line model [46] is used for initial design of the ACMPA elements of the reflectarray. Figure 2.2 presents the transmission line model for the ACMPA shown in Figure 2.1. The patch antenna in Figure 2.1 can be basically modeled by two radiating slots separated by a low impedance transmission line. Each radiating slot is modeled by the impedance Y_s which is given by

$$Y_s = G_s + jB_s \tag{2.1}$$

where G_s represents the radiation conductance and B_s models the stored energy in the stray field of the open circuit at the planes $x = \pm L_p/2$. The accurate formulation for G_s and B_s are given in [51] where the expressions are calculated by taking into account the following points;

- ✓ The width of the patch (W_p) may differ from the resonant wavelength.
- ✓ The effect of mutual couplings between two slots at planes $x = \pm L_p/2$.

- ✓ The radiation due to the side walls at the planes $y = \pm W_p / 2$.

In the analysis of the transmission line model, one of the most challenging parts is to obtain transformation ratios n_1 and n_2 accurately. There are invalid approximations in the literature as in [50] which are refuted by [46].

The transformation ratio n_1 of the first transformer modeling the coupling between the patch antenna and the aperture on the ground plane is given as [46]

$$n_1 = \frac{L_a}{2W_{peff}} \tag{2.2}$$

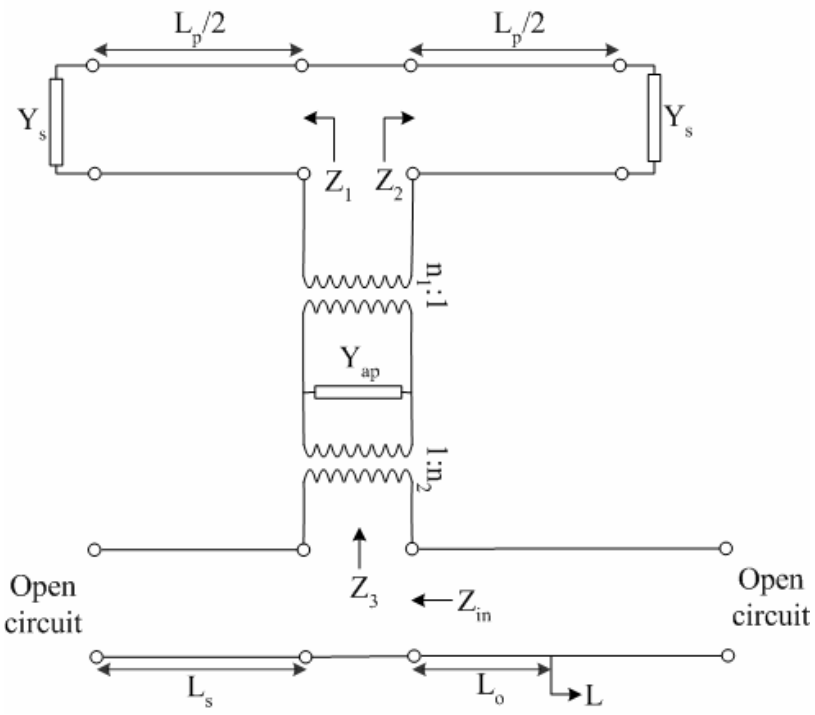

Figure 2.2: Transmission line model of the aperture coupled microstrip patch antenna.

In (2.2), L_a is the length of the slot line and W_{peff} is the effective width of the patch antenna calculated by taking into account the stray field [51].

The second transformation ratio n_2 modeling the coupling of the aperture to the microstrip line below the feed substrate is given by the following expression [46]:

$$n_2 = \left[2G(w) - G(w+l) - G(w-l)\right] / 2\pi wl \tag{2.3}$$

$$G(\alpha) = \left(1-\alpha^2\right)\left(\tan^{-1}\alpha\right) + \alpha\left(\ln\left(1+\alpha^2\right)\right) \tag{2.4}$$

$$w = W_m / 2h_f \tag{2.5}$$

$$l = L_a / 2h_f \tag{2.6}$$

where W_m is the width of the microstrip line and h_f is the thickness of the feed substrate shown in Figure 2.1.

Then the impedance Z_3 in the transmission line model shown in Figure 2.2 is calculated as

$$Z_3 = \frac{n_2^2}{n_1^2\left(Y_1 + Y_2\right) + Y_{ap}} \tag{2.7}$$

The aperture admittance Y_{ap} in (2.7) is obtained from two short circuited, parallel connected slot lines. The equation for Y_{ap} is

$$Y_{ap} = -j\frac{2}{Z_{ca}\cot(k_a L_s/2)} \tag{2.8}$$

The characteristic impedance Z_{ca} and the wave number k_a of the slot line are calculated by full-wave simulations carried out in HFSS. Moreover, the closed form

calculations for Z_{ca} and k_a in (2.8) can be obtained by applying modifications on Cohn's method [52] and considering the effect of the patch antenna on the slot line [53].

Hence, the equation for Z_{in} is given as

$$Z_{in} = \frac{n_2^2}{n_1^2(Y_1 + Y_2) + Y_{ap}} - jZ_c \cot(\beta L_s) \tag{2.9}$$

where Z_c is the characteristic impedance and β is the propagation constant of the open circuited matching stub of length L_s.

The general design procedure can be summarized as follows;

- ✓ The antenna and feed substrate is chosen considering the bandwidth, efficiency, cost, availability and suitability to the production process.
- ✓ The expression $Y_3 = \frac{1}{Z_3} = \frac{n_1^2(Y_1 + Y_2) + Y_{ap}}{n_2^2}$ is obtained from (2.7), and the real part of the expression $\frac{n_1^2(Y_1 + Y_2)}{n_2^2}$ is tried to be made equal to the characteristic admittance of the microstrip line Y_c by playing with the dimensions of the patch antenna and the length of the aperture. Again one should pay attention to get reasonable dimensions such that the length of the aperture (L_a) is not too long or short according to the width (W_p) of the patch antenna.
- ✓ Then the width of the aperture (W_a) is chosen such that the imaginary part of the expression $\frac{n_1^2(Y_1 + Y_2)}{n_2^2}$ is compensated by the aperture admittance Y_{ap}.
- ✓ Finally, the length of the open circuited stub L_s is set to the quarter wavelength at the frequency of interest to obtain the matching.

- ✓ If the aperture width (W_a) is restricted by the etching tolerances of the production technology or it turns unreasonably out to be too high, then appropriate dimension for (W_a) is chosen and the patch dimensions are adjusted such that the real part of Z_3 is equal to Z_c. Then the imaginary part of Z_3 is cancelled by playing with the length of the matching stub L_s.

In order to prove the validity of the transmission line model, an aperture coupled microstrip patch antenna with dimensions shown in Figure 2.3 is matched to the free space at 26.5 GHz in HFSS. Pyrex (ε_r = 4.6, *Loss Tangent* = 0.005, *Thickness* = 0.5 mm) is used as an antenna and feed substrate. To calculate the reflection factor at the $x = 0$ plane, the wave port shown in Figure 2.3 is deembeded by a distance 2.83 mm and S-parameters are renormalized with respect to 80 ohm which is the characteristic impedance of the transmission line of width 0.4 mm on the Pyrex substrate. Finally the reflection coefficient of the ACMPA is obtained as shown in Figure 2.4 in HFSS.

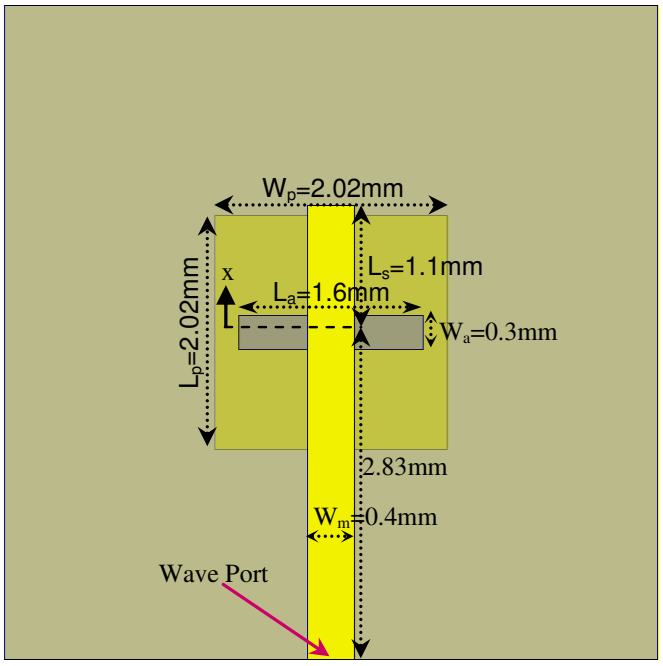

Figure 2.3: An ACMPA matched to the free space at 26.5 GHz in HFSS.

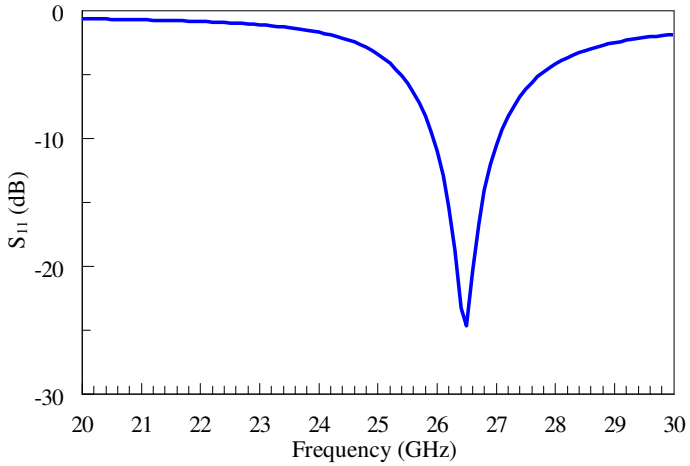

Figure 2.4: The 80 ohm reflection factor (S_{11}) of the antenna shown in Figure 2.3.

The reflection factors (S_{11}) renormalized to 80 ohm obtained from the HFSS simulations of the ACMPA in Figure 2.3 and its transmission line equivalent circuit are compared in Figure 2.5. It is seen that the transmission line circuit gives input impedance value close to that of calculated by HFSS at the resonant frequency of 26.5 GHz. As the frequency deviates from the resonant frequency the accuracy of the transmission line circuit decreases.

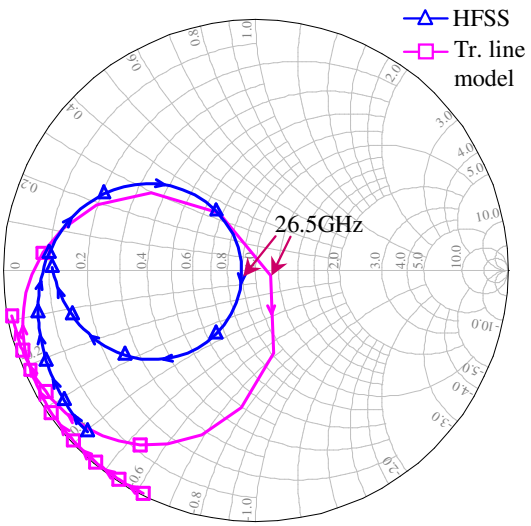

Figure 2.5: Comparison of the 80 ohm reflection factors (S_{11}) obtained from HFSS and transmission line model.

Hence, it is seen that transmission line equivalent circuit is a good approximation around the center frequency of the ACMPA and it can be used to calculate the antenna dimensions roughly at the initial design. Then the fine tuning to obtain perfect matching can be done by applying a slight change to the antenna dimensions and simulating at the full wave EM simulator.

The effects of the parameters in the ACMPA structure described by Pozar in [54] are as follows:

- ✓ Lower dielectric constant for the antenna substrate results in higher bandwidth, wider steering range without scan blindness and lower surface wave excitation which increases the radiation efficiency.
- ✓ As the thickness of the antenna substrate increases, the bandwidth is also increases but the coupling to the aperture decreases.
- ✓ The length of the microstrip patch antenna is highly effective in the determination of the resonant frequency.
- ✓ The radiation resistance of the patch antenna can be decreased by increasing the width of the patch. But the square patches results high cross polarization levels and but they can be used in the applications where dual or circular polarization is required.
- ✓ The phase shift for a given transmission line length can be increased by using higher dielectric constant materials as a feed substrate but the substrate loss increases.
- ✓ When the thickness of the feed substrate decreases, the fields are more confined to the substrate and the back radiation decreases but the substrate loss increases. If the losses due to thinner substrate are compensated by decreasing the back radiation losses then the thinner substrate can be used to increase the coupling level of the transmission line to the aperture.
- ✓ As the aperture length increases the coupling to the transmission line also increases but if the slot length is chosen higher than the required for the matching the back radiation increases due to the high power transfer.

- ✓ The aperture width is also effective in the coupling to the transmission line but not much effective as the aperture length. It should be chosen just large enough to provide coupling.
- ✓ The width of the transmission line determines the characteristic impedance and the phase delay for a given transmission line length. Thinner transmission line couples more to the aperture. But it should be chosen so that it is physically realizable.
- ✓ In order to obtain the maximum coupling, the aperture should be centered both relative to the patch antenna and the transmission line. The angle between the aperture and the transmission line should also be 90°.
- ✓ The length of the matching stub is usually chosen slightly less than the quarter wavelength to include the open end effect. But this is the case if the impedance seen from the aperture by the transmission line is purely real and the length of the matching stub can be different from the quarter wave length if required for the impedance matching. As the length of the matching stub is increased from the quarter wavelength, the smith chart plot of the impedance locus versus frequency of ACMPA shifts to the inductive region.

CHAPTER III

REFLECTARRAY DESIGN

The design of reflectarray is examined in two sections. Section 3.1 explains the main steps in designing reconfigurable reflectarray composed of ACMPA by discussing the effects of possible RF MEMS switch types and nonideal phase design curve. Then, Section 3.2 presents the design, production, and measurement results of a prototype reflectarray to prove the design concept.

3.1. RECONFIGURABLE REFLECTARRAY DESIGN

The aim of the reflectarray is to direct the electromagnetic field from a feed antenna (usually horn) to a desired direction by choosing proper reflection phase values of the electromagnetic field for each element in the array [4]. Figure 3.1 shows the reflectarray antenna and its feed. In order to obtain an equiphase plane of the reflected field, the distance from phase center of the feed antenna to the unit element (R_i) and from unit element to the plane that is desired to be the equiphase plane of the reflected field ($\bar{r}_e.\bar{r}_r$) are calculated. Then these distances are multiplied by the free space (the medium is generally free space) propagation constant (k_0) and the total phase delay due to the propagation of the wave at free space is calculated for each element. Then total phase delay from feed to the equiphase plane at any path is made equal to $2\pi N$ as in (3.1) by choosing required reflection phase values (Ψ_i) for each element.

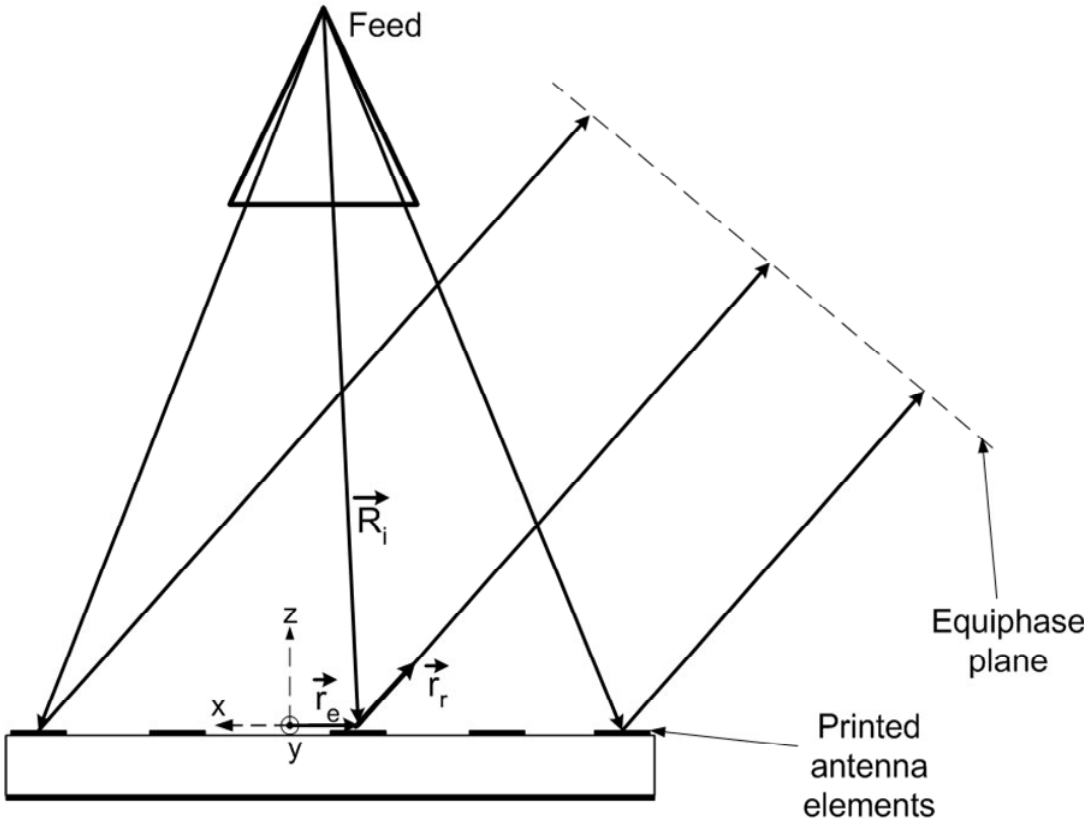

Figure 3.1: General design procedure of the reflectarray.

$$-k_0\left(R_i + \bar{r}_e.\bar{r}_r\right) + \psi_i = 2\pi N \tag{3.1}$$

The design procedure can also be interpreted from another point of view. The phase values due to the path from feed to the unit cell are compensated by choosing proper phase values for each element (Ψ_{il}) such that all the reflected field at the reflectarray surface have the same phase value. This means, the reflectarray radiates to the broadside. Then the progressive phase shift is calculated from well known array theory [2] by considering the angle at which the reflected main beam is desired to be directed. Finally, constant progressive phase shift is added to each reflection phase value (Ψ_{il}) and final reflection phase values (Ψ_i) are obtained.

The variation in the phase of the reflection coefficient is satisfied by making changes in the geometrical structure of the phase shifting element of the individual unit cell. In the design of the reflectarray, it is critical to obtain the phase design curve, which is the plot of the phase of the reflection coefficient versus the geometrical dimension that is varied in the phase shifting element. In order to scatter the field with the desired phase, different approaches have been developed such as microstrip patches with stubs of variable length [55]-[57] and dipoles or patches of variable size [58], [59] as discussed in Section 1.1. In this study, a reconfigurable reflectarray is designed so that the phase of the scattered field will be controlled by inserting variable length microstrip transmission line coupled to the patch by means of an aperture in the ground plane as shown in Figure 3.2.

3.1.1. Phase Design Curve

In general, to design a reflectarray, the first step is to obtain reflection phase characteristics with respect to a parameter of the array geometry (such as size of the patch, length of the transmission line etc.), namely, phase design curve [4], [60]. The reflectarray composed of ACMPA uses the transmission line at the feed substrate as a phase shifting geometry.

The main difficulty in obtaining phase design curve is to take into account the mutual couplings. That is, how the reflection phase versus the phase shifter geometry graph will be affected by the existence of the neighboring elements. Constructing the array structure and measuring the whole array to obtain phase design curve is impractical. Furthermore, it is also not practical to construct the whole array in the simulation environment because simulating the whole array is time consuming or impossible for large arrays. In order to solve this problem, it can be assumed that the array is infinite so that the solution in the unit cell is obtained using periodic array Green's function. In HFSS simulations, proper boundary conditions at the boundaries of the unit cell are developed.

The ACMPA matched to the free space at 26.5 GHz in Section 2.2 is used to calculate the phase design curve of the reflectarray. To obtain the phase design curve, the unit cell structure shown in Figure 3.2 is constructed in HFSS. Then the unit cell is made an infinite array by the proper boundary conditions at the boundaries. There are three methods in obtaining an infinite array.

First method is to use periodic boundary conditions in HFSS by assigning one boundary as a master and its opposing as a slave boundary. That is, Boundary1 in Figure 3.2 is assigned as a Master1 and Boundary3 is assigned as Slave1. Similarly, Boundary2 is assigned as Master2 and Boundary4 is assigned as Slave2. In HFSS, the Slave boundary takes the same field value as its corresponding Master boundary and hence, an infinite array is virtually constructed as shown in Figure 3.3. Then the array is fed by the *x*-polarized plane wave incident on the patch antennas. The reflection phase and magnitude of the plane wave at the intentionally inserted plane (this is usually the top face of the air region lying above the unit cell) are calculated by the help of field calculator in HFSS.

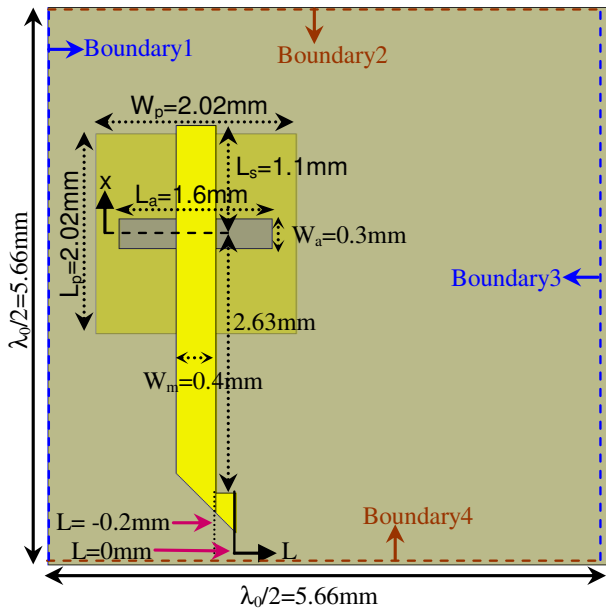

Figure 3.2: The unit cell structure of the reflectarray.

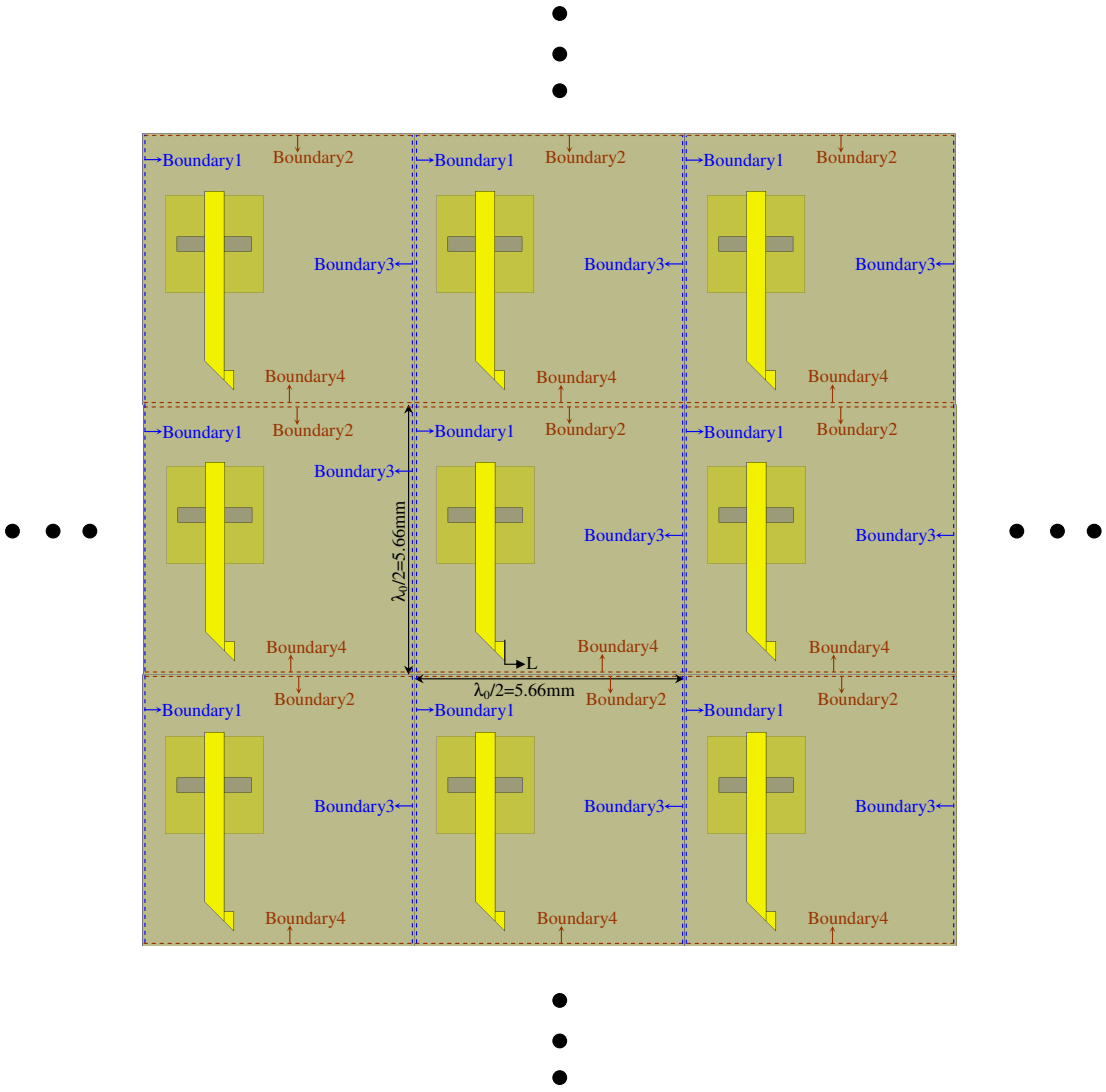

Figure 3.3: A virtual infinite array constructed with Master and Slave boundaries.

The second method is to assign either perfect electric (perfect-E) or perfect magnetic (perfect-H) planes at the opposing boundaries. If Boundary2 and Boundary4 in Figure 3.2 are assigned as perfect electric walls then the tangential electric fields will be zero at the perfect-E boundaries. Similarly, Boundary1 and Boundary3 are assigned as perfect magnetic walls and then the tangential magnetic field will be zero at the perfect-H boundaries. Then the structure is excited by a wave port such that the polarization of the E-field is in x-direction and the phase of S_{11} is measured. Due to

the image theory, the virtual but not symmetric infinite array will be occupied for the ACMPA as shown in Figure 3.4. This can be accounted as follows. An *x*-polarized plane wave which meets the boundary conditions at the perfect-E and perfect-H boundaries will be received by the patch antenna. The electromagnetic power coupled to the transmission line through the aperture will be reflected back to the patch antenna due to the open end at the transmission line. Then the reflected field will be constructed by the current distribution on the top surface of the unit cell.

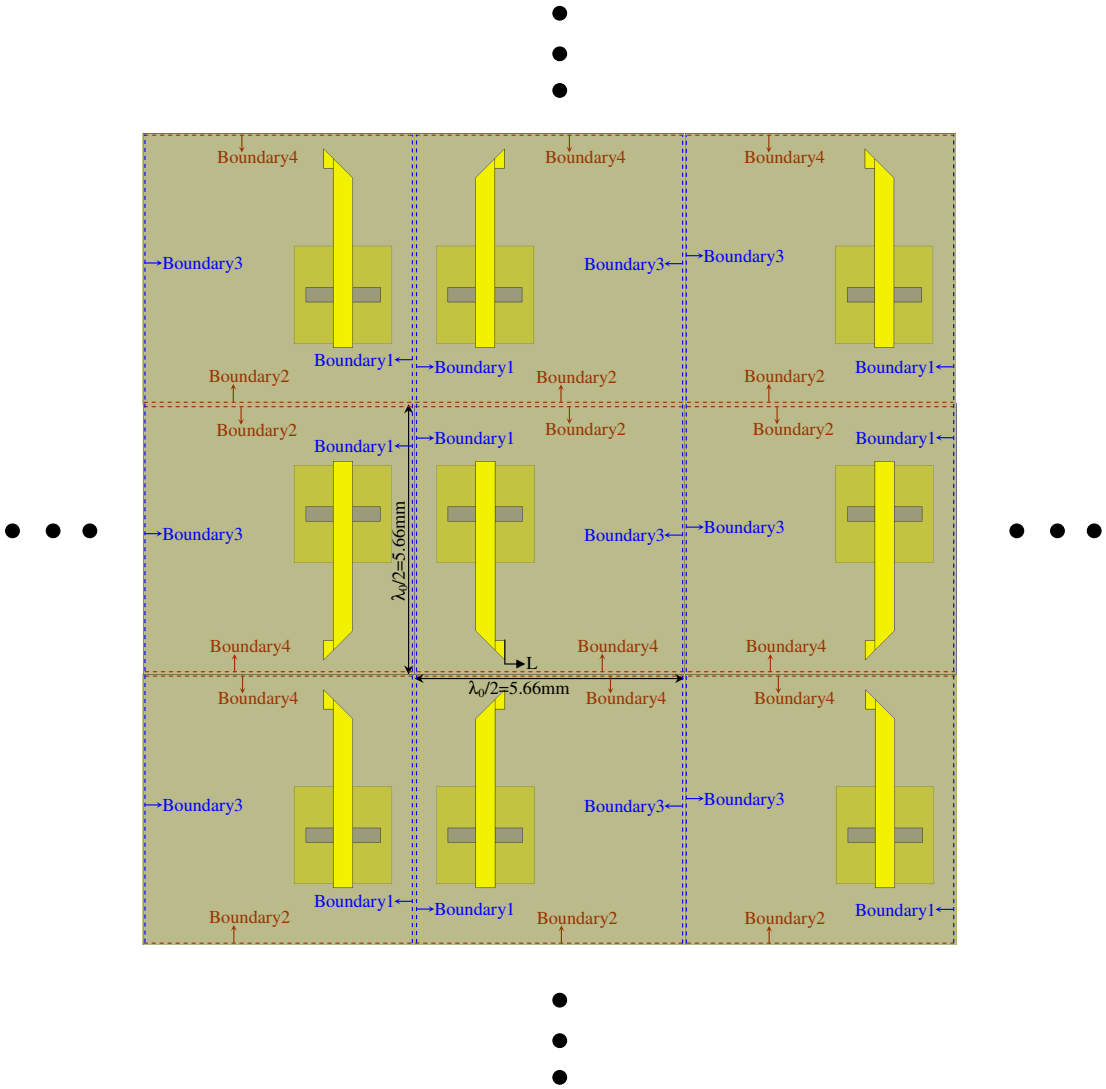

Figure 3.4: A virtual infinite array constructed with perfect-E and perfect-H planes at the boundaries.

Similarly, the back radiation field will be constructed by the top surface of the unit cell. That is, the shape of the metallic structure (patch antenna) determines the existence of the current at the surface. If we consider Figure 3.5 (a) and (b) the triangular shape representing the conducting part carrying currents at the numbered points. The directions of the currents are shown by the arrows at the points. When there is a perfect electric wall, then the image of the real currents at the plane vertical to the perfect electric wall will have the same magnitude and direction with the image current at the opposite side of the perfect-E plane. The real current and its image have the same vertical distance to the perfect-E plane. Hence bilateral symmetry of the triangular shape is obtained but the currents at the points on the image triangle are out of phase with respect to the currents on real triangle if we consider the shape of the conducting surface. Similarly, in the case of a perfect-H plane shown in Figure 3.5 (b), both the real and image currents at the points will have the same direction and hence there will a bilateral symmetry of the triangular shape with respect to the perfect-H plane with the image currents in phase with the real currents. In conclusion, the perfect-E and perfect-H planes can be used to obtain undistorted infinite array if the unit cell geometry has a bilateral symmetry at its principal planes as in [61].

The third method is the waveguide simulator method [62]. This method is used by drawing and simulating the real waveguide together with the unit cells in HFSS. The unit cell dimension is chosen such that the one unit cell or an integer multiples of unit cells fits to the waveguide aperture or the waveguide is built by considering the dimensions of the unit cell if possible at the frequency of interest. In HFSS, all of the unit cell or set of unit cell boundaries are chosen as perfect-E planes to construct a waveguide. The elements are placed at the end of the waveguide and the waveguide is excited by a wave port. Then the phase of S_{11} is measured. Again this method can be used if the unit cell geometry has a bilateral symmetry at its principal planes to obtain undistorted virtual infinite array [63].

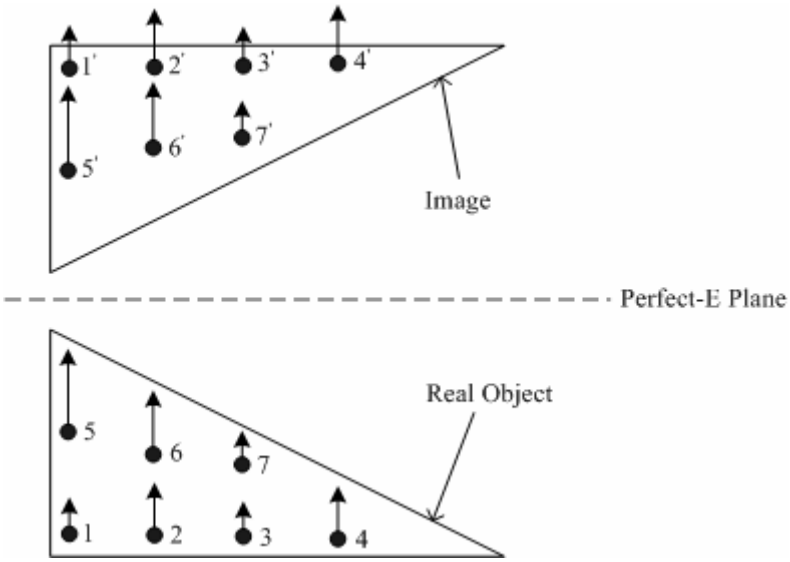

(a)

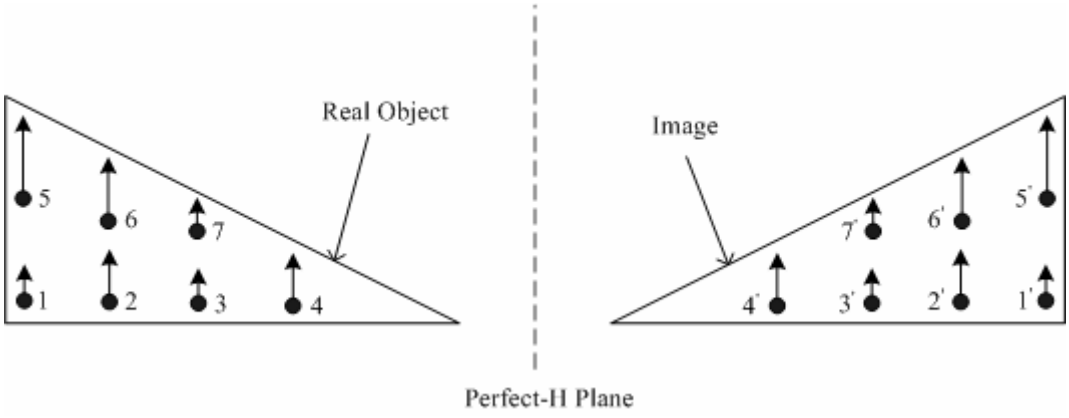

(b)

Figure 3.5: The illustration of the image theory in the case of (a) perfect-E and (b) perfect-H planes.

The unit cell structure shown in Figure 3.2 has no bilateral symmetry and for this reason the first method is used to obtain the reflection phase characteristics. The phase design curve at 26.5 GHz obtained for the unit cell of the reflectarray is shown in Figure 3.6. It can be seen that the curve is nonlinear between 1mm<*L*<2.5mm. Linearity of the phase design curve is an important parameter such that it simplifies

the calculation of the transmission line lengths. Once the required reflection phase values are calculated for each element, the corresponding transmission line lengths can be calculated easily by dividing the phase values to the slope of the linear phase design curve. The other parameter that affects the performance of the reflectarray is the sensitivity of the phase design curve [60]. If the sensitivity of the curve is high then the reflection phase values are affected much by the inaccuracies in the production of the phase shifter part. This is the case where there is a sharp change in the phase design curve.

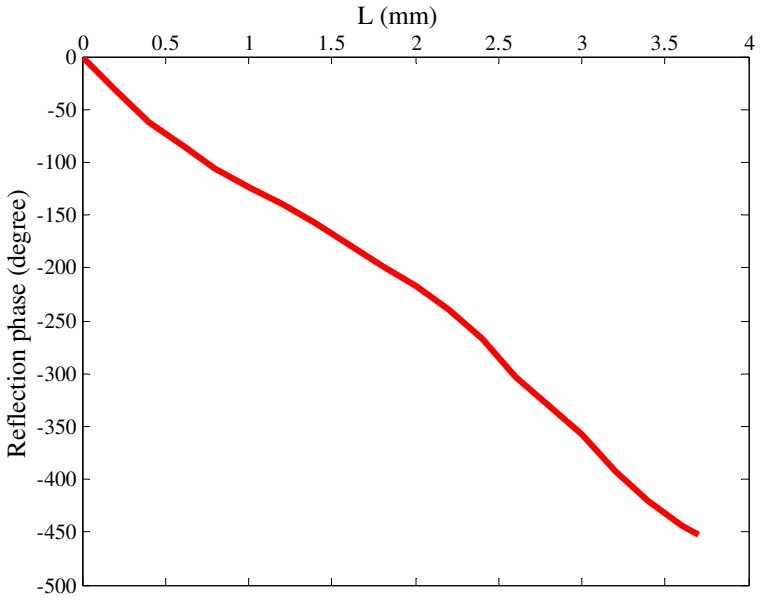

Figure 3.6: The phase design curve of the unit cell structure shown in Figure 3.2.

3.1.2. Reflection Phase Calculation for the Reconfigurable Unit Cells

The reconfigurable aperture coupled microstrip reflectarray includes RF MEMS switches to change the lengths of the transmission lines at the phase shifter part in the unit cell element shown in Figure 3.7. The reconfigurable reflectarray is fed by a

horn antenna and the required values of L for each element are calculated from the required phase values to reflect the beam to the desired direction [4]. In this study, a reflectarray is designed to switch the main beam between broadside and 40° at 26.5GHz. Hence two different L values are required for each element in the reflectarray and the RF MEMS switch is used to switch between two L values resulting in change in the direction of the main beam. Before discussing the values of the required L values, i.e. the reflection phase values at the phase shifter part, the nonlinearity of the phase design curve shown in Figure 3.6 is eliminated.

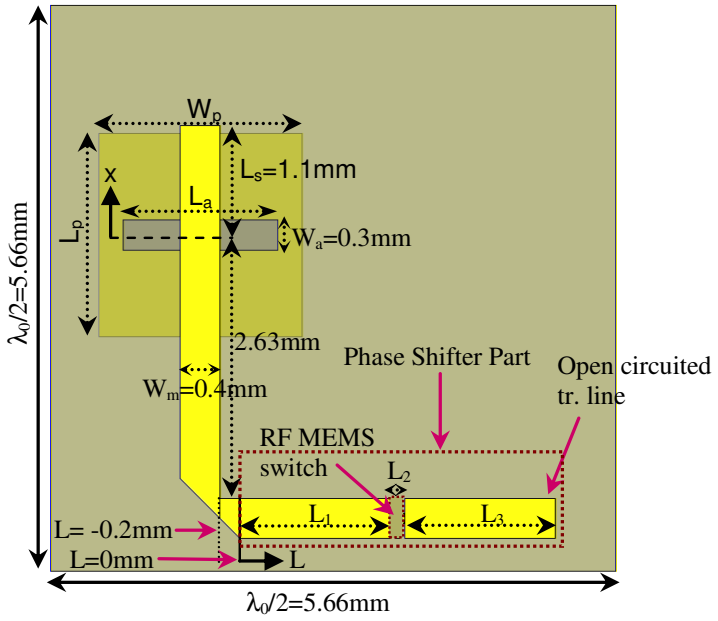

Figure 3.7: The unit cell structure with the reconfigurable phase shifter part.

As the first step, aperture coupled microstrip patch antenna with dimensions given in Table 3.1 was matched to the free space as discussed in Section 2.2. The glass substrate with thickness h_p=h_f=0.5mm and dielectric constant ε_{rp}= ε_{rf}=4.6 is used as an antenna and transmission line substrate. Then the unit cell composed of the first antenna configuration (Antenna1 in Table 3.1) is simulated by inserting master and slave boundary conditions at the borders in the commercial EM simulation tool

HFSS by Ansoft. The element spacing is half a wavelength in both directions. The unit cell is excited with a linearly polarized plane wave considering the polarization of the patch antenna and the phase of the reflected field is evaluated by the help of field calculator in HFSS for each value of *L* incremented in the direction shown in Figure 3.7 without the phase shifter part. Hence, the phase design curve, which is a graph of the reflection phase as a function of the length of the transmission line is obtained for the configuration Antenna1 and given in Figure 3.8. Since the transmission line of the ACMPA is incremented only in one direction and the other part is used as a matching stub with length L_s, there is large space for the transmission line to be incremented at the phase shifter part. Thus we can obtain a large phase swing which is many times of 360° and this increases the bandwidth [19] of the reflectarray. Then the ideal transmission line on glass substrate with W_m=0.4mm is simulated in HFSS and compared with the phase design curve obtained from the first antenna configuration. It is seen in Figure 3.8 that the phase design curve and the ideal curve for the first antenna configuration does not follow each other well. By playing with the dimensions of the first antenna configuration, the phase design curve can be made closer to the ideal simulation [64]. The second antenna configuration parameters of which are shown in Table 3.1 is obtained by applying a slight change in the size of the patch antenna and the aperture of the first antenna configuration. The phase design curve of the second antenna configuration fits well with the ideal curve as shown in Figure 3.8.

Table 3.1: ACMPA dimensions used in the reconfigurable design (all dimensions are in mm).

	W_p	L_p	W_a	L_a	W_m	L_s
Antenna1	2.02	2.02	0.3	1.6	0.4	1.1
Antenna2	2.03	2.03	0.3	1.55	0.4	1.1

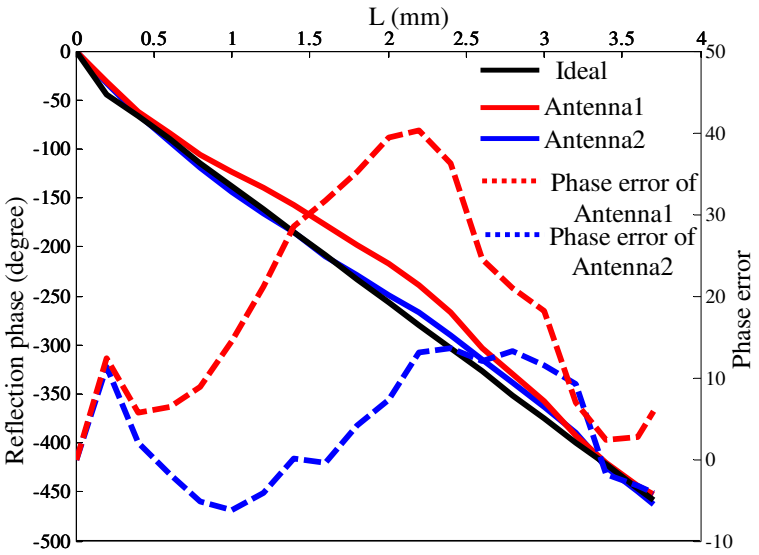

Figure 3.8: The comparison of the phase design curves of two different antenna configurations with the ideal curve.

Two different sets of L values which are L_1 and $L_1+L_2+L_3$ in Figure 3.7 determined from the phase design curve of the second antenna configuration are shown in Table 3.2 and Table 3.3, respectively. The set of L_1 values directs the main beam to broadside while the set of $L_1+L_2+L_3$ values are used to rotate the beam to 40°. The difference between the two sets of transmission line values, i.e. L_2+L_3, shown in Table 3.4 indicates the constant progressive phase shift in the array. In order to convert the negative values in Table 3.4 to positive, the transmission line length of 2941µm indicating the phase shift of 360° is added to the $L_1+L_2+L_3$ values in Table 3.3 where necessary in the array. Hence the main beam is desired to direct the main beam to broadside and 40° for the shorter and longer values of the transmission lines respectively.

Table 3.2: The set of transmission line lengths, i.e. L_1 in Figure 3.7, in the array to direct the beam to broadside (all dimensions are in μm).

Rows \ Columns	1	2	3	4	5	6	7	8	9	10
1	878	1020	1128	1198	1234	1235	1199	1127	1020	878
2	1615	1759	1867	1939	1975	1975	1939	1866	1758	1615
3	2324	2470	2579	2652	2688	2689	2652	2578	2469	2324
4	64	211	322	396	433	433	396	321	211	63
5	715	864	977	1051	1088	1088	1051	976	864	715
6	1336	1487	1600	1676	1714	1714	1676	1600	1487	1336
7	1926	2079	2193	2270	2308	2308	2270	2193	2079	1926
8	2484	2638	2754	2831	2869	2870	2831	2753	2638	2484
9	68	224	340	418	457	457	418	340	223	68
10	559	715	833	911	951	951	912	833	715	559

Table 3.3: The set of transmission line lengths, i.e. $L_1+L_2+L_3$ in Figure 3.7, in the array to direct the beam to broadside (all dimensions are in μm).

Rows \ Columns	1	2	3	4	5	6	7	8	9	10
1	878	1965	77	1093	2074	79	988	1862	2700	562
2	1615	2704	816	1834	2815	819	1728	2601	497	1299
3	2324	474	1528	2547	587	1533	2441	372	1208	2008
4	64	1156	2212	290	1273	2218	185	1056	1891	2688
5	715	1809	2867	946	1928	2873	840	1711	2544	399
6	1336	2432	549	1571	2554	558	1465	2335	226	1020
7	1926	83	1142	2164	207	1152	2059	2928	818	1610
8	2484	642	1703	2726	768	1714	2620	547	1377	2168
9	68	1169	2230	313	1297	2242	207	1075	1903	2693
10	559	1660	2723	806	1791	2736	701	1568	2395	243

Table 3.4: The difference between the two sets of transmission line values, i.e. L_2+L_3 (all dimensions are in μm).

Rows \ Columns	1	2	3	4	5	6	7	8	9	10
1	0	945	-1051	-105	840	-1156	-211	735	1680	-316
2	0	945	-1051	-105	840	-1156	-211	735	-1261	-316
3	0	-1996	-1051	-105	-2101	-1156	-211	-2206	-1261	-316
4	0	945	1890	-106	840	1785	-211	735	1680	2625
5	0	945	1890	-105	840	1785	-211	735	1680	-316
6	0	945	-1051	-105	840	-1156	-211	735	-1261	-316
7	0	-1996	-1051	-106	-2101	-1156	-211	735	-1261	-316
8	0	-1996	-1051	-105	-2101	-1156	-211	-2206	-1261	-316
9	0	945	1890	-105	840	1785	-211	735	1680	2625
10	0	945	1890	-105	840	1785	-211	735	1680	-316

The RF MEMS series switch shown in Figure 3.10 are inserted between two transmission lines for the reasons explained in Section 3.1.3 to change transmission line length. However, the series switch does not sustain pure isolation of the transmission lines and when the value of L_3 is increased for the up state of the series switch, the reflection phase changes as in Figure 3.9 which is not desirable. This effect is not tolerable when the value of L_3 is between 2300μm and 2800μm which is the case for the columns 4, 7, and 10 in Table 3.4 after adding the transmission line length of 2941μm to the values in Table 3.3 where necessary to make all the values in Table 3.4 positive. Hence, the transmission line length of 2941μm is added to the values in Table 3.3 except columns 4, 7, and 10. Furthermore, it is subtracted from the 4^{th} and 9^{th} row of column 10 and all the values in Table 3.4 becomes positive except the 4^{th}, 7^{th}, and 10^{th} column. Thus, the reflection phase values will be given for the broadside when the series switches at the columns 4, 7, and 10 are in down state while switches at the other columns are in up state and for the 40°, all the switches change their state. Since the reflection phase values are affected from length L_3 for the up state of the series switch, the final values of L_1 and L_3 need to be altered for the fine tuning of the phases. This is done by iteratively simulating the phase

shifter part which is separated from the reflectarray to save the simulation time. The final results for the phase shifter lengths some of which are bended in order not to cross the neighboring elements are shown at the APPENDIX B.

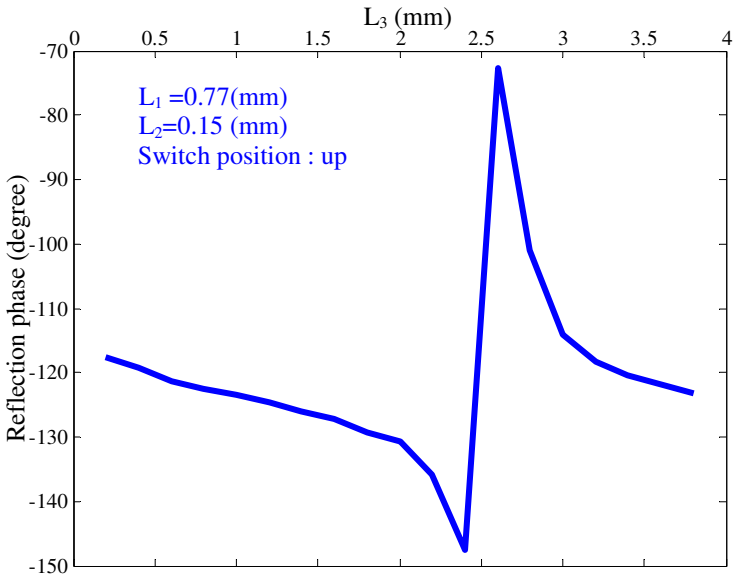

Figure 3.9: The reflection phase characteristics of the phase shifter with series switch.

3.1.3. Possible RF MEMS Switch Types

Two types of RF MEMS switches are investigated to change the length of a transmission line; series and shunt configurations. Series RF MEMS switch is the bridge structure between two transmission lines. When the switch is in down position it connects two physically separated transmission lines named as Tr. Line1 and Tr. Line2 as shown in Figure 3.10. The *s*-parameters of the series RF MEMS switch are given in Figure 3.11. The insertion loss of the switch is better than -0.5dB and isolation is less than -10dB which are acceptable at the frequency of interest.

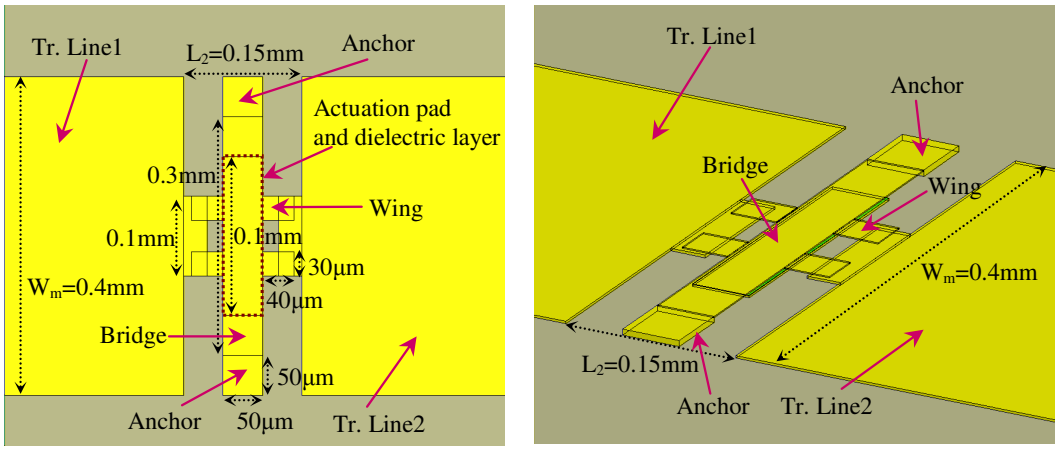

(a) (b)

Figure 3.10: (a) The top and (b) the perspective views of the series switch.

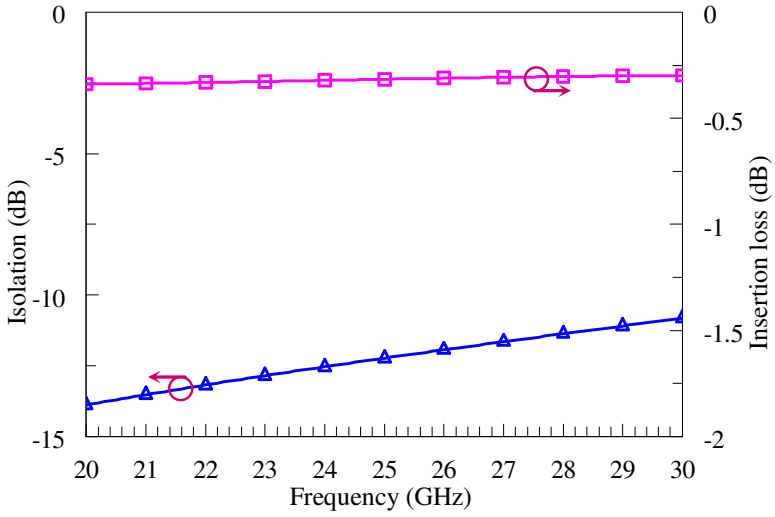

Figure 3.11: The *s*-parameters of the series switch.

However, the better isolation can be achieved with shunt RF MEMS switch shown in Figure 3.12, where the bridge is connected to an open circuited radial stub of quarter wavelength at the frequency of interest and hence the bridge is shorted. In the shunt

switch configuration, Tr. Line1 and Tr. Line2 are not physically separated. When the bridge is in down state, the transmission line couples to the bridge via the dielectric layer due to the high capacitance between them and the transmission line is shorted. Hence Tr. Line1 and Tr. Line2 are electromagnetically separated form each other. The *s*-parameters of the shunt RF MEMS switch are shown in Figure 3.13. The insertion loss of the shunt switch is almost the same as the series switch but the isolation of the shunt switch is much better than series switch at 26.5GHz. However, shunt switch has low bandwidth in terms of isolation characteristics and this may affect the reflectarray performance. Besides, shunt switch covers a large area due to its open circuited radial stub and introduces mutual coupling. Furthermore, choosing series switch can be seen reasonable in terms of its isolation because it connects two transmission lines and one of them is open circuited. Hence, the isolation of the series switch is not so effective in terms of power loss because the power will be reflected back at the open circuit and the losses are caused only by the dielectric losses and the radiation losses.

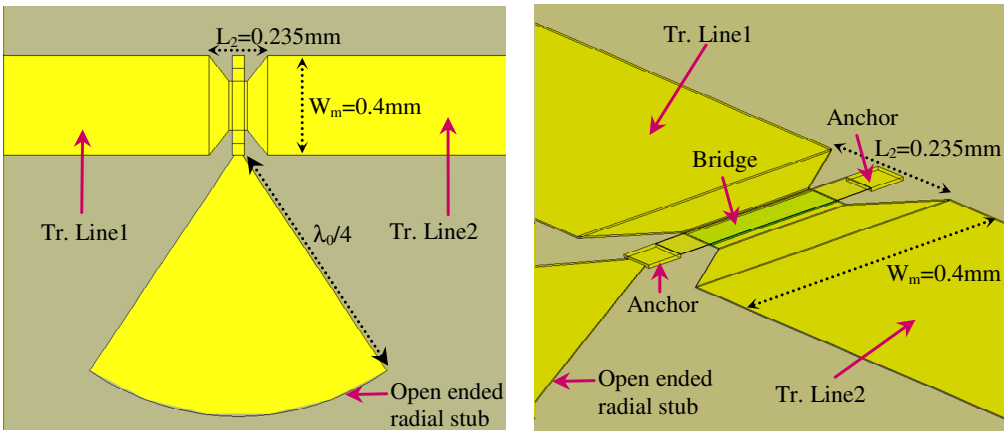

(a) (b)

Figure 3.12: (a) The top and (b) the perspective views of the shunt switch.

The series and shunt switch phase shifter structures are placed at the phase shifter part in the reflectarray constructed with second antenna configuration as shown in Figure 3.7. Then reflection phases are calculated for the dimensions and switch positions of the series and shunt switches shown in Table 3.5 and Table 3.6 respectively. Then the respective reflection phase values are marked at the phase design curve of the second antenna configuration in Figure 3.14. It is seen that the series switch configuration follows the phase design curve better than the shunt switch configuration. The reason for the difference of the reflection phase values for shunt switch configuration is the mutual couplings due to the open circuited radial stub covering large area. Hence the series switch configuration shown in Figure 3.10 is chosen in the unit cell of the reconfigurable reflectarray antenna operating at 26.5GHz.

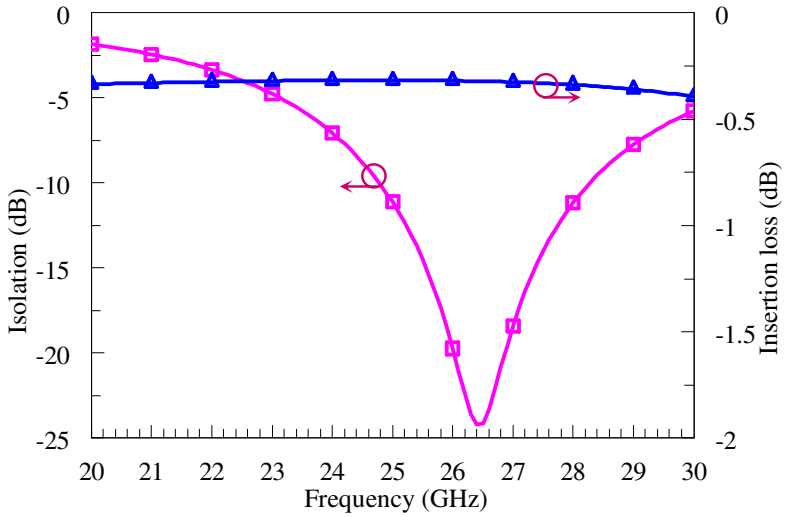

Figure 3.13: The *s*-parameters of the shunt switch.

Table 3.5: The phase shifter with series switch dimensions for which the reflection phases are calculated at Figure 3.7.

L_1 (mm)	L_3 (mm)	Bridge Position
0.75	0.75	up
1	0.35	up
1.25	0.5	up
1.5	1.5	up
1	0.35	down
1.25	0.5	down
1.5	1.5	down

Table 3.6: The phase shifter with shunt switch dimensions for which the reflection phases are calculated at Figure 3.7.

L_1 (mm)	L_3 (mm)	Bridge Position
1	0.35	up
1.25	0.5	up
1.5	1.5	up
0.75	0.75	down
1	0.35	down
1.25	0.5	down
1.5	1.5	down

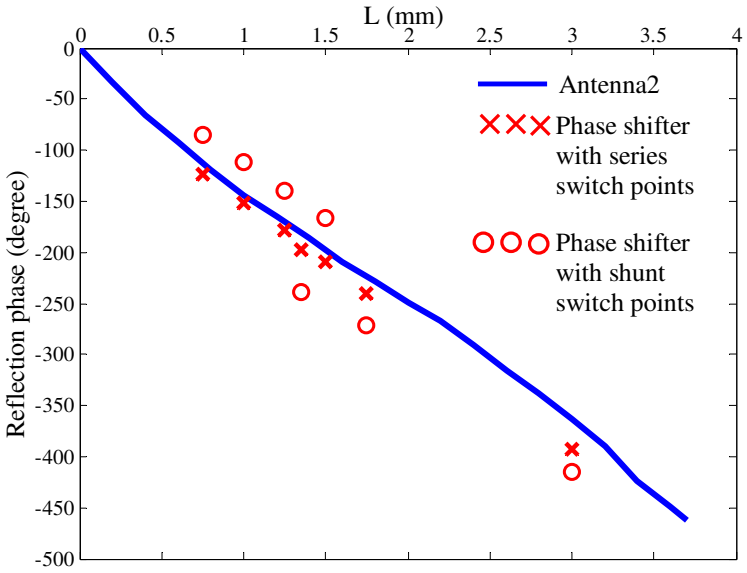

Figure 3.14: Comparison of the phase values calculated by using the series and shunt RF MEMS switches at the phase shifter part and phase design curve of the second antenna configuration.

3.2. PROTOTYPE DESIGN

The prototype of 20x20 aperture coupled microstrip patch reflectarray with the required transmission line lengths to rotate the beam to 40° is designed and produced on a Rogers Duroid without RF MEMS switches to validate the concept of beam switching reflectarray. The transmission line model is used to match an ACMPA to the free space at 25GHz shown in Figure 3.15 which is used as a unit cell of the prototype reflectarray. The element spacing is half wavelength in both directions. All the reflectarray elements have the same patch antenna and aperture dimensions except the transmission line length *L* in Figure 3.15. The phase design curve for the unit cell shown in Figure 3.16 is obtained using periodic boundary conditions as discussed in Section 3.1.1. The phase design curve is almost linear which simplifies the calculation of the transmission line lengths from the phase values such that it is possible to express the transmission line lengths as a linear function of the reflection

phase values. Furthermore, it includes the effects of the mutual couplings due to neighboring elements as if elements are in infinite array.

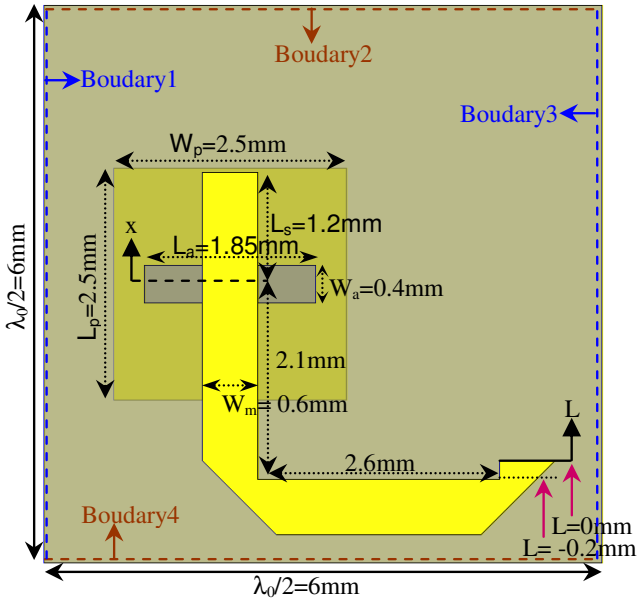

Figure 3.15: The unit cell structure of the prototype reflectarray.

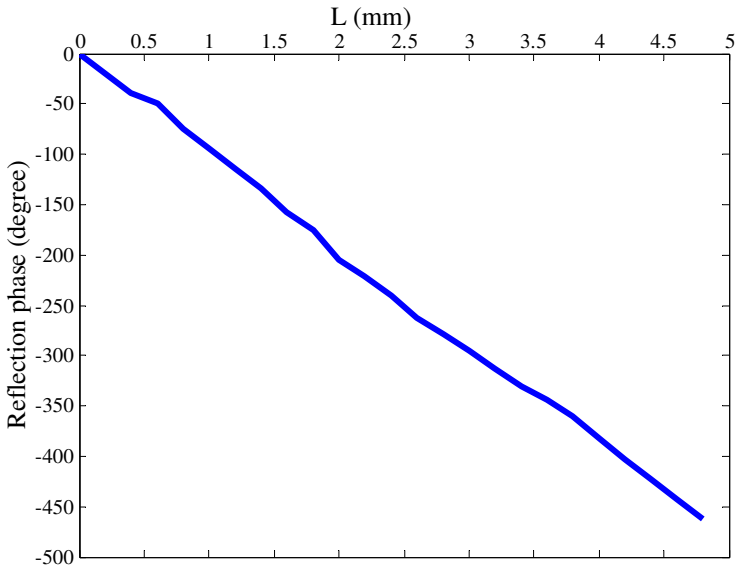

Figure 3.16: The phase design curve of the unit cell structure shown in Figure 3.15.

The prototype reflectarray is designed to be fed by a horn antenna such that the phase center of the horn antenna is fixed relative to the center of the reflectarray as shown in Figure 3.17. The feed horn antenna is positioned to sustain almost uniform amplitude distribution over the reflectarray surface. Then the paths between each unit element and the phase center of the horn antenna are calculated. Hence, the phase values of incident field for each element are determined. These phase values are compensated by choosing proper transmission line lengths using phase design curve shown in Figure 3.16 for each element to give required phase shift to reflect the electromagnetic field to 40° in H-plane.

The designed reflectarray is produced using Printed Circuit Board (PCB) technology. Reflectarray consisting of microstrip patch antennas of length L_p=2.5mm and width W_p=2.5mm is printed on Rogers4003(ε_{rp}=3.38) materials with thickness h_p=0.51mm. An aperture with dimensions of length L_a=1.85mm and width W_a=0.4mm on the ground plane at the backside of the antenna substrate is constructed to sustain the coupling between the patch antenna and the transmission line with dimensions W_m=0.4mm and L_s= 1.2mm on the feed substrate. Both the antenna and feed substrates are Rogers4003(ε_r = 3.38, *Loss Tangent* = 0.0027, *Thickness* = 0.51mm). Then both substrates are screwed together and measured in an anechoic chamber. The measurement results shown in Figure 3.18 are in a good agreement with the simulated data. The difference between the simulation and measurement may be due to nonuniform amplitude distribution on the array and diffraction from the truncated ground plane and substrate. The measurement results for different frequencies shown in Figure 3.19 indicate that the main beam deflects from 40° by an angle of 2° in 2GHz band. The detailed discussion on the measurement techniques of reflectarrays are given in APPENDIX A.

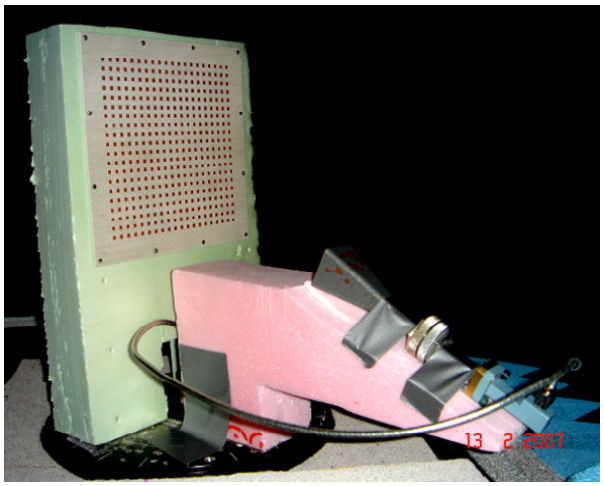

Figure 3.17: Measurement set up of the prototype reflectarray antenna.

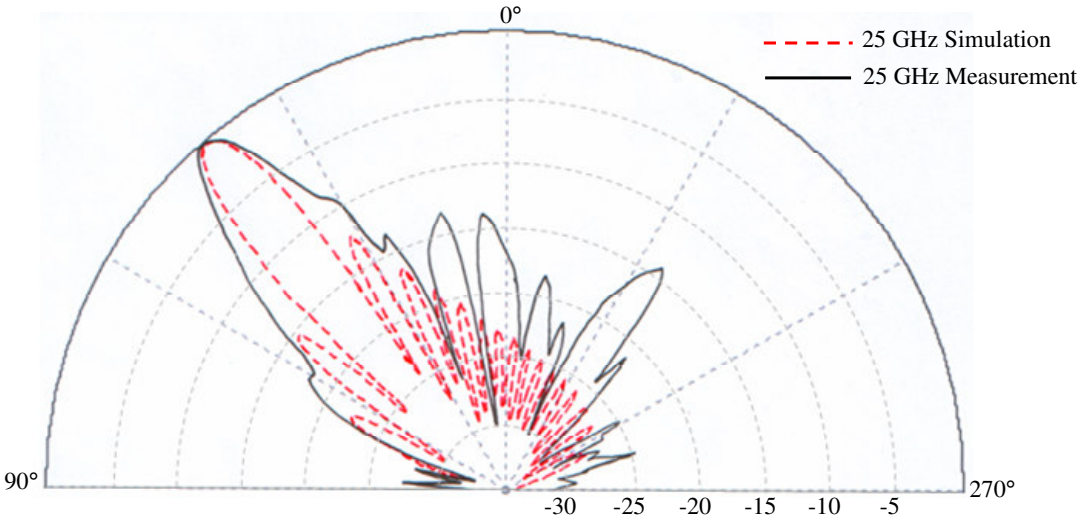

Figure 3.18: Measurement result of the prototype antenna.

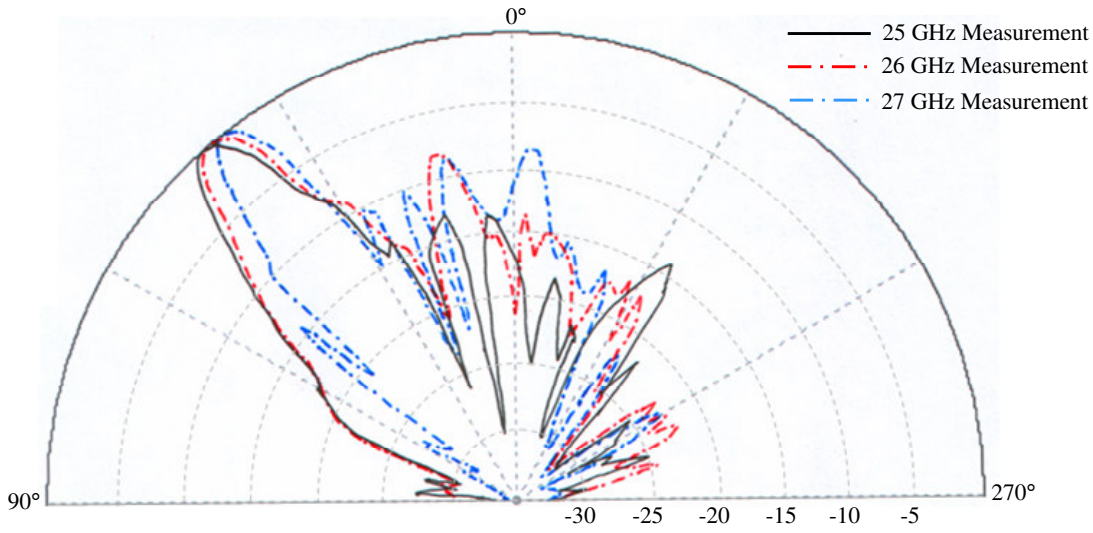

Figure 3.19: Measurement results of the prototype antenna carried out at diffrerent frequencies.

CHAPTER IV

FABRICATION OF THE RECONFIGURABLE REFLECTARRAY

In this chapter, the production method of the reconfigurable reflectarray is examined. The bias lines of the switches are inspected in terms of mutual couplings in Section 4.1. A possible way of integrating the wafer bonding step to the standard surface micromachining process already developed at the Middle East Technical University Microelectronic Facilities (METU-MET) for the producing various RF MEMS switches is introduced in Section 4.2.

4.1. LAYOUT DRAWING

After the prototype measurements, design of reflectarray with RF MEMS switches has been finalized and masks were drawn as shown in Figure 4.1. As can be seen in the layout drawing, the final reflectarray will have two signal lines. SIGNAL1 is used to actuate the RF MEMS switches at the columns 2, 3, 5, 6, 8, 9 while SIGNAL2 actuates the switches at the columns 4, 7 and 10. As discussed in Section 3.1.2, SIGNAL1 and SIGNAL2 actuate their switches in an opposite manner. That is, when switches connected to SIGNAL1 are in up state, the switches connected to a SIGNAL2 are in down state or vice versa.

The standard geometry is tried to be obtained for the bias lines of the RF MEMS switches to keep the simplicity in the layout drawing. As can be seen in Figure 4.2,

there are two main parallel bias lines composed of sputtered gold passing through at the middle of two neighboring columns. The bias line at the right is used for the grounding the switch at the right column while bias line at the left is used for carrying the actuation signal to the bridge at the left column. The bias lines constructed from the sputtered gold (Au) is connected to the resistive bias lines composed of sputtered Si-Cr at an average distance of 1500μm before the switch. By this method, the mutual couplings introduced by the interaction of the Au bias lines and the transmission line of the switch is avoided.

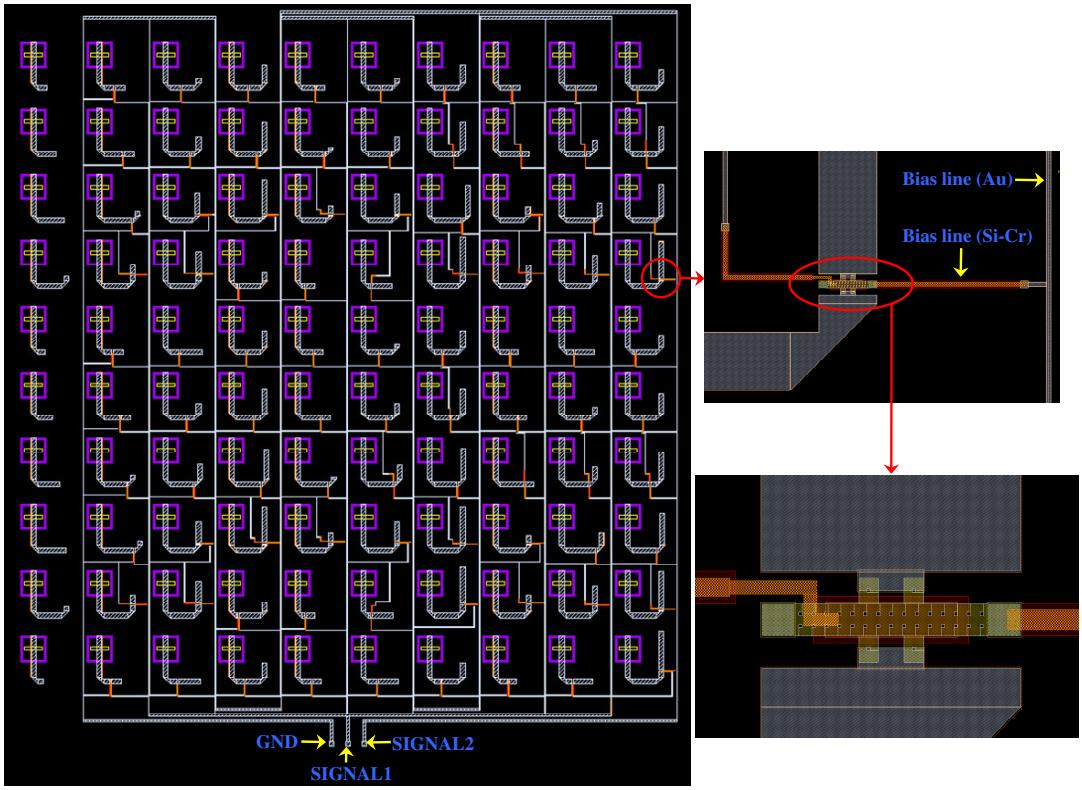

Figure 4.1: Mask layout of 10x10 Reflectarray with RF MEMS swicthes.

In order to see the effects of the bias lines on the phase design curve, the unit cell structure designed for the construction of the reconfigurable reflectarray in Section 3.1.2 is drawn with the bias lines (Au) in HFSS as shown in Figure 4.2. The

widths of the bias lines are chosen to be 30μm for the safe etching in the construction of the bias lines. Then the structure is made an infinite array by using the periodic boundary conditions in HFSS and the phase design curves are calculated for different spacing *S* values between two main bias lines. The simulation results shown in Figure 4.3 indicate that the bias lines (Au) whose closest distance to the transmission line is 1000μm for *L* = 1215μm in the simulation do not significantly disturb the phase design curve. The biggest deviation occurs for *S* = 20μm and 3.2μm<*L*<3.7μm. Therefore, the main bias line spacing is chosen to be 15μm by considering that the 10μm spacing is too small for the safe production.

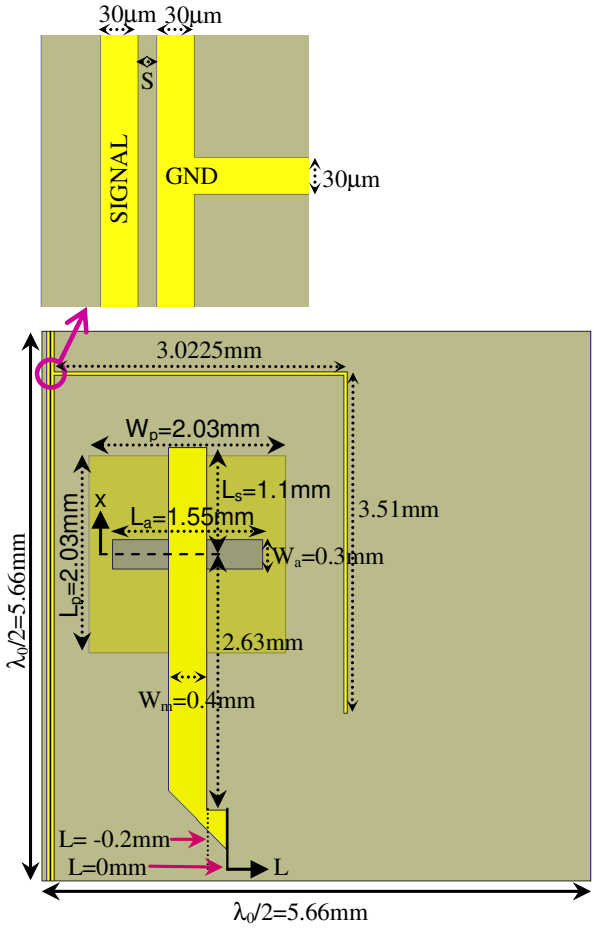

Figure 4.2: The unit cell structure of the reconfigurable reflectarray with gold bias lines.

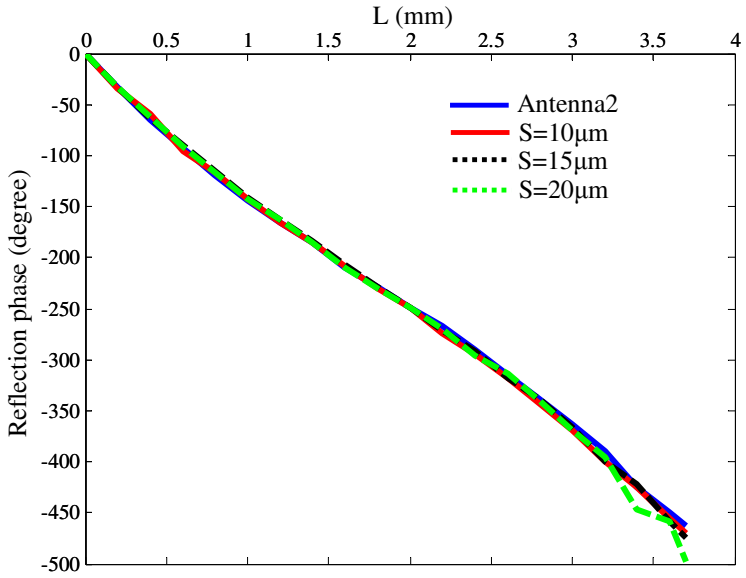

Figure 4.3: The effects of different spacing between the bias lines on the phase design curve.

4.2. PROCESS FLOW

The Scanning Electron Microscopy (SEM) image of the typical shunt RF MEMS switch produced using the standard surface micromachining process developed at the Middle East Technical University Microelectronic Facilities (METU-MET) is shown in Figure 4.4. The basic standard process shown in Figure 4.5 is as follows. Initially the first metallization is constructed by sputtering the gold metal. Then the gold is electroplated on the first metallization. The first metallization is etched to get the transmission line geometry. After that, the support layer called sacrificial layer is deposited on the shaped first metallization. The gold is again sputtered on the sacrificial layer to form a second metallization. Then the second metal is shaped by etching to get the bridge structure. Finally, the sacrificial layer is removed by the release process and bridge becomes free to move in up and down direction.

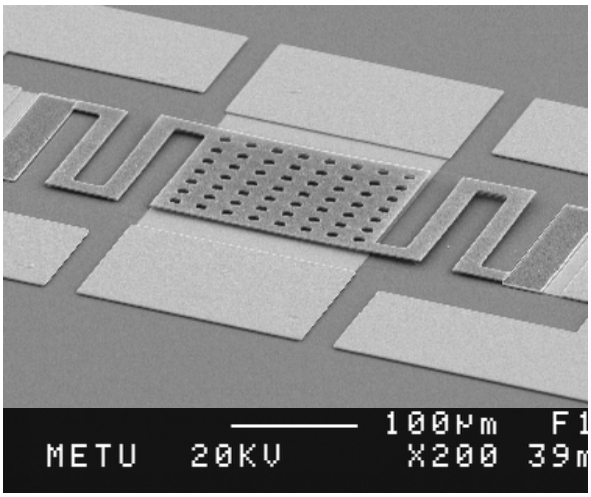

Figure 4.4: The SEM photo of the RF MEMS switch.

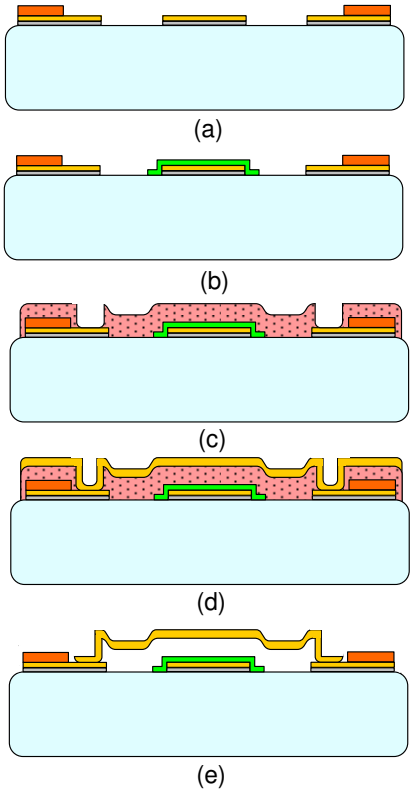

Figure 4.5: Standard process flow developed at METU-MET for the production of the RF MEMS switch.

The standard surface micromachining process briefly described above needs to be improved for the production of the designed reconfigurable reflectarray in the sense that the reflectarray composed of ACMPA contains two substrates (antenna and feed substrates) and they must be bonded at some stage of the production of the RF MEMS switches. The bonding stage is decided to be realized at the beginning of the process due to the following reasons. First, bonding two wafers after the construction of the RF MEMS switches is not reasonable because the high temperature at the bonding phase will possibly induce stress on the structural layer or even the bridge structures will be destroyed by the physical force applied to the two wafers for good bonding. Furthermore, patterning the first metallization at the antenna substrate to construct the patch antennas after the bonding will also destruct the gold layers at the feed substrate because the etching is achieved by wet etchants. For these reasons, the wafer bonding phase will be realized as the first stage of the process. Then the patch antenna formation will be completed at the antenna substrate and the patch antennas will be protected from the gold etchants by thick titanium layer. Then the standard surface micromachining process will be followed to construct the transmission lines and switches at the feed substrate. Two 500μm-thick Pyrex 7740 glass substrates (ε_r=4.6, *tan* δ=0.005) will be used as an antenna and feed substrate.

The switch side of the symbolic reconfigurable reflectarray antenna is shown in Figure 4.6. The detailed process flow is described in Figure 4.7, Figure 4.8 and Figure 4.9 using the cross section views in Figure 4.6 as follows:

In the first step of the process flow shown in Figure 4.7, both of the wafers will be (a) coated with gold and (b) patterned to construct the aperture on ground plane. (c) Then both wafers will be bonded at the aperture sides to have a common ground plane and aperture. (d) Then the Ti and Au will be sputtered to form a fist metallization at the other side of the antenna substrate. Then first metallization at the antenna substrate will be patterned to construct patch antennas. (e) Finally, the antennas will be covered with sputtered thick Ti layer for protection.

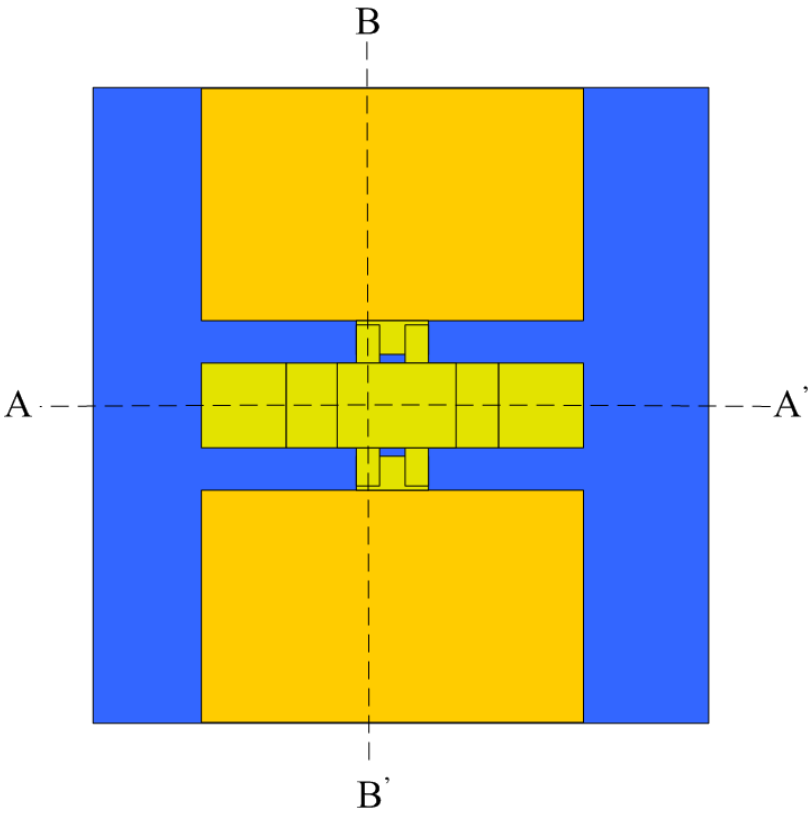

Figure 4.6: The switch side of the reconfigurable reflectarray structure composed of aperture coupled microstrip patch antennas where the construction steps are described in Figure 4.7, Figure 4.8, Figure 4.9.

In the second step shown in Figure 4.8, the first metal and the dielectric layers for the switch structures are processed by first (a) depositing the 2000-Å thick Si-Cr resistive layer by sputtering and patterning by wet etching. (b) The next is the sputtering of a 100/3000-Å thick Ti/Au layer, which is required as the seed layer for electroplating of the base metallization. (c) The base metallization layer is formed using a 2-µm thick gold layer, which is electroplated inside the regions defined by the mold photoresist. (d) The remaining Ti/Au seed layer is etched using wet etching with selective titanium and gold etchants. (e) A 3000 Å-thick Si_3N_4 layer is coated as

the DC isolation layer using plasma enhanced chemical vapor deposition technique (PECVD) and patterned using the reactive ion etching (RIE) technique.

The final step shown in Figure 4.9 starts with the (a) spin-coating of the photodefinable polyimide, PI 2737, as the 2-μm thick sacrificial layer. (b) Then the polyimide is patterned and etched at the anchor regions of the bridge. (c), (d) After that, a 1-μm thick gold layer is sputter-deposited and patterned as the structural layer. Then, the thick Ti layer over the patch antennas is etched. (e) Finally, the sacrificial layer is wet etched in the SVC-175 photoresist stripper, rinsed in IPA, and dried in a supercritical point dryer.

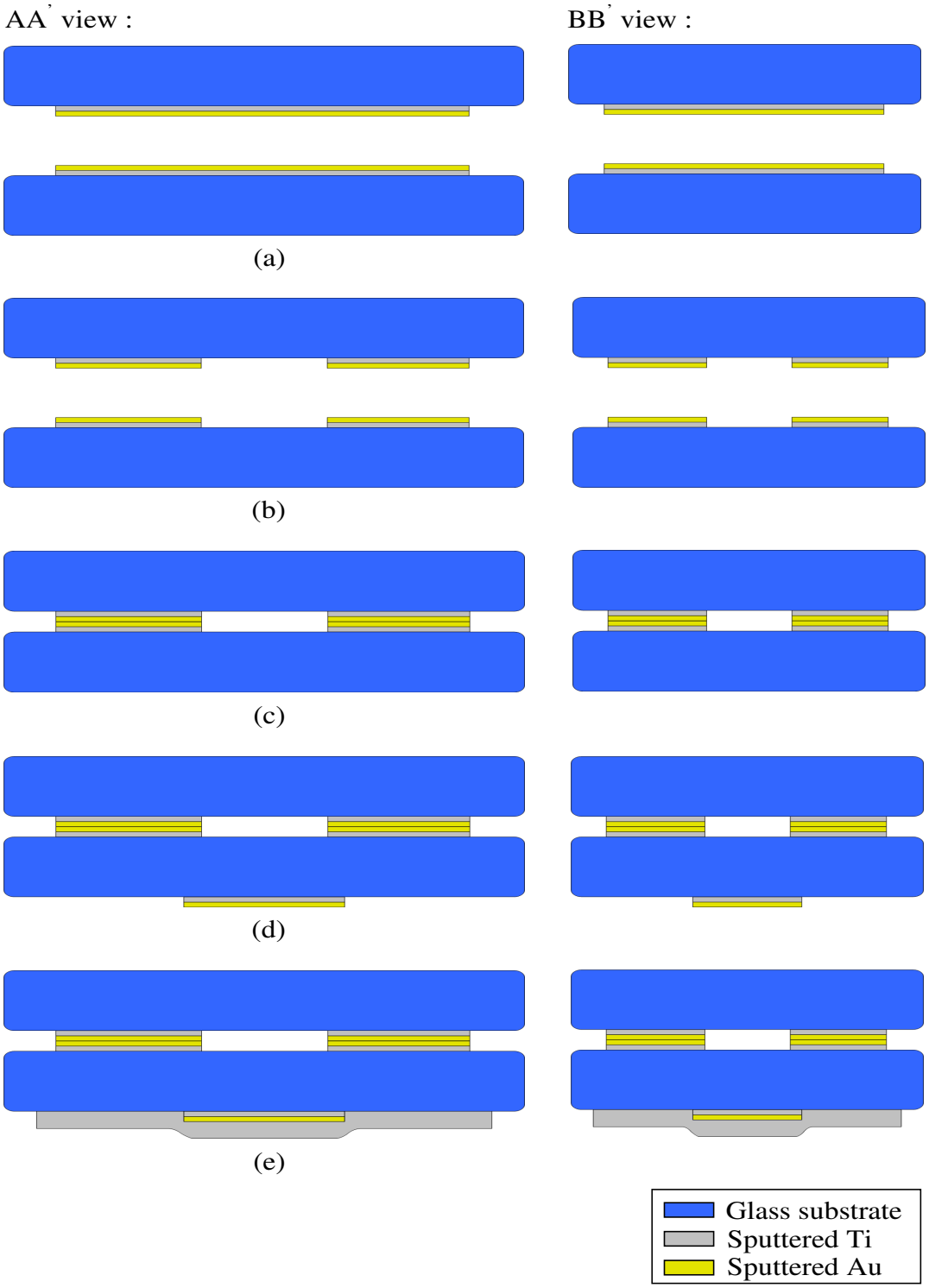

Figure 4.7: Reconfigurable reflectarray process flow of (a) first metallization (ground plane formation), (b) first metal patterning, (c) wafer bonding, (d) first metallization and patterning (patch antenna formation), and (e) thick Ti layer deposition.

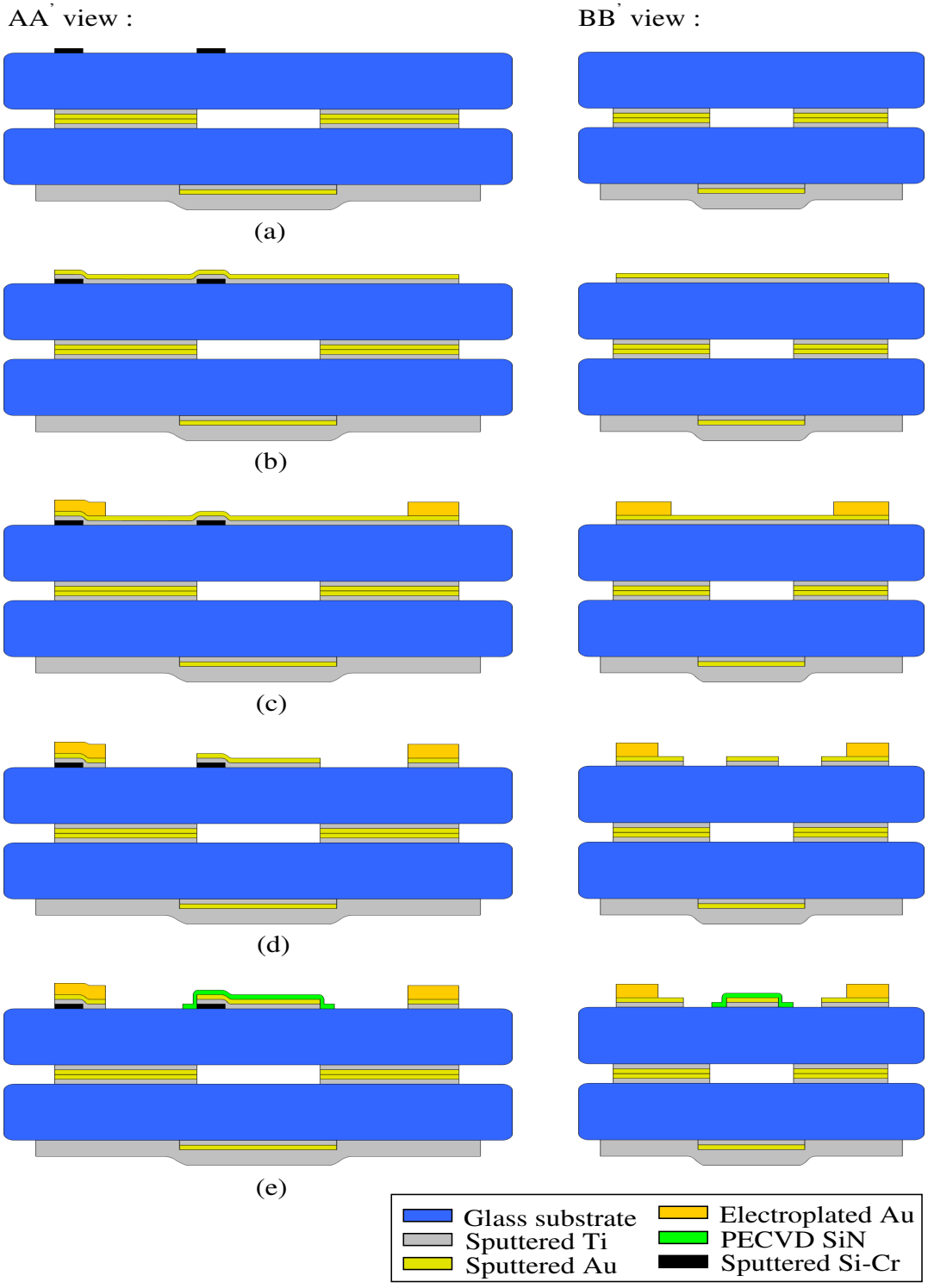

Figure 4.8: Reconfigurable reflectarray process flow of (a) Si-Cr resistive layer formation, (b) first metallization, (c) gold electroplating, (d) first metallization patterning, and (e) SiN deposition and patterning.

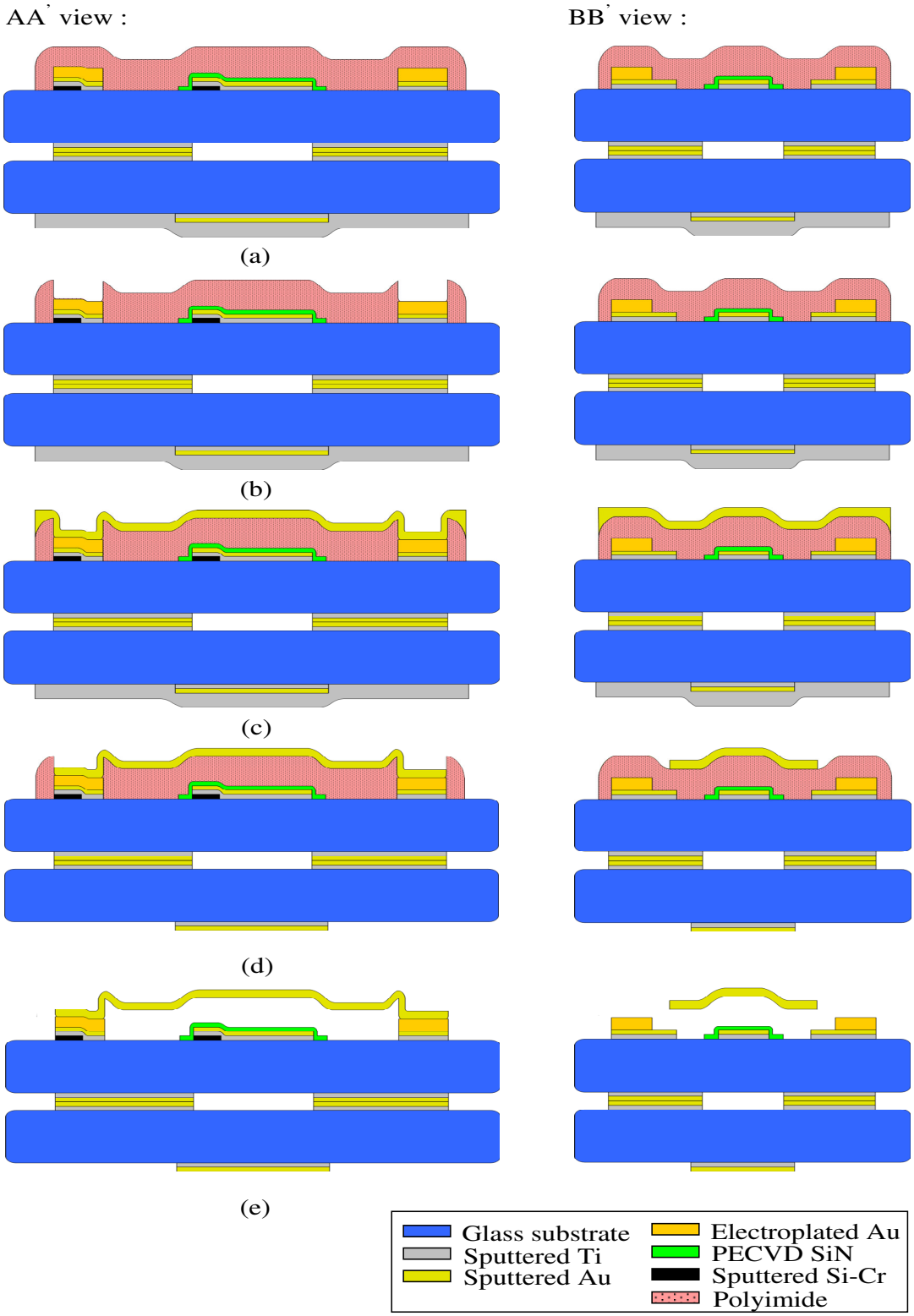

Figure 4.9: Reconfigurable reflectarray process flow of (a) polyimide deposition, and (b) patterning, (c) second metal deposition, (d) second metal patterning, (e) release.

CHAPTER V

CONCLUSIONS AND FUTURE WORK

In this thesis, the design of 10x10 reconfigurable reflectarray antenna is presented at 26.5GHz where the beam is switched between the broadside and 40° from broadside by series RF MEMS switches. The aperture coupled microstrip patch antenna (ACMPA) configuration is chosen as a reflectarray element due to the advantages mentioned in Section 2.1. The reconfigurable reflectarray consists of 100 ACMPA elements each having one series RF MEMS switches in their transmission lines except the first column resulting a total of 90 RF MEMS switches. When the production of the designed reflectarray is completed, it will be one of the few examples of the monolithic reconfigurable reflectarray in the literature that employs large number of RF MEMS switches distributed over the large wafer area.

The design of the reflectarray starts with the transmission line analysis of the ACMPA used to match the antenna to the free space. Then the infinite array structure is formed from the matched ACMPA using the proper boundary conditions in HFSS and the array is illuminated by a plane wave. The reflection phase values are calculated by incrementing the transmission line length and the phase design curve indicating the reflection phase values versus transmission line length is obtained. The effect of the mutual couplings on the phase design curve is taken into account using the infinite array structure in the simulations. The phase errors due to the nonlinear and nonideal phase design curve are reduced using HFSS. Then two sets of transmission line lengths are determined from the phase design curve to rotate the main beam to the broadside and 40°. After that the series RF MEMS switches are inserted into the transmission lines to sustain the switching between two angles. The

mutual couplings introduced by the RF MEMS switches and their bias lines are eliminated by a proper design using HFSS. Finally, the transmission lines with RF MEMS switches are simulated iteratively to obtain the fine tuning of the phases.

The prototype of 20x20 aperture coupled microstrip patch reflectarray without RF MEMS switches is designed at 25GHz with the required transmission line lengths to rotate the beam to 40° and produced using Printed Circuit Board (PCB) technology to validate the concept of beam switching reflectarray. The measurement results of the prototype reflectarray show that the main beam can be rotated to 40° as desired.

Based on the conclusions drawn in this section, the future works can be summarized as follows:

- The reconfigurable reflectarray designed in thesis will be produced using standard surface micromachining process at the Middle East Technical University Microelectronic Facilities (METU-MET).
- The number of RF MEMS switches in the phase shifter of the reconfigurable reflectarray designed in this thesis can be increased to switch between more than two angles.
- Different phase shifter structures that provide larger phase shifts per unit length can be designed.
- With the design of proper phase shifter geometry having many RF MEMS switches, 360° of phase delay can be covered and the behavior of the phase shifter becomes closer to the analog phase shifter than a digital one. Hence, steering the beam of the reflectarray becomes possible rather than switching the beam.
- The back radiation in the ACMPA can be blocked by inserting a ground plane above the transmission lines which eliminates the radiation losses of the reflectarray.

REFERENCES

[1] D. G. Berry, R. G. Malech, and W. A. Kennedy, "The Reflectarray Antenna," *IEEE Transactions on Antennas Propagation.*, vol. AP-11, pp. 645-451, Nov. 1963.

[2] C. Balanis, "Antenna Theory: Anaylsis and Design," *New York: Wiley*, 1997.

[3] C. S. Malagisi, "Microstrip Disc Element Reflectarray," *Electron. Aerospace Syst. Conv.*, Sep. 1978.

[4] D. M. Pozar, S. D. Targonski, and H.D. Syrigos, "Design of Millimeter Wave Microstrip Reflectarrays," *IEEE Transactions on Antennas and Propagation*, vol. 45, no. 2, pp. 287-296, Feb. 1997.

[5] C. Apert et al. "ERASP: A New Reflectarray Antenna for Space Applications," *EuCAP 2006*, Nice, France, Nov. 2006.

[6] D. M. Pozar, S. D. Targonski, and R. Pokuls, "A Shaped-Beam Microstrip Patch Reflectarray," *IEEE Transactions on Antennas and Propagation*, pp. 1167 - 1173, July 1999.

[7] J. A. Encinar, L. Datashvili, H. Baier, M. Arrebola, M. Sierra-Castaner, J. L. Besada, H. Legay, and G. Toso, "Breadboard of a Three-Layer Printed Reflectarray for Dual Polarisation and Dual Coverage," *28th ESA Antenna Workshop on Space Antenna Systems and technologies*, Noordwijk, The Netherlands, June 2005.

[8] J. A. Zornoza, R. Lebber, J. A. Encinar, W. Menzel, "Folded Multi-Layer Microstrip Reflectarray with Shaped Pattern," *IEEE Transactions on Antennas and Propagation,* vol. 54, no. 2, pp. 510-518, Feb. 2006.

[9] J. Huang, R. Hodges, M. Zawadzki, S. Rengarajan, C. Han, and K. Chang, "Recent Development of Printed Reflectarrays at JPL," *International Union of Radio Science (URSI)* Ghent, Belgium, Oct-2005.

[10] Wolfgang Menzel, Dietmar Pilz, and Maysoun Al-Tikriti, "MM-Wave Folded Reflector Antennas with High Gain, Low Loss, and Low Profile," *IEEE AP Magazine*, pp. 24 – 29, June 2002.

[11] T. Metzler and D. Schaubert, "Scattering from a Stub Loaded Microstrip Antenna," *Antennas and Propagation Society International Symposium*, AP-S. Digest, pp. 446 - 449, June 1989.

[12] D. M. Pozar and T. A. Metzler, "Analysis of a Reflectarray Antenna Using Microstrip Patches of Variable Size," *Electronics Letters*, vol. 29, no. 8, pp. 657-658, April 1993.

[13] D. M. Pozar and S. D. Targonski, "A Microstrip Reflectarray Using Crossed Dipoles," *IEEE Antennas and Propagation Society International Symposium*, pp. 1008-1011, June 1998.

[14] J. A. Encinar, "Design of Two-Layer Printed Reflectarrays Using Patches of Variable Size," *IEEE Transactions on Antennas and Propagation*, vol. 49, no. 10, pp. 1403-14010, Oct. 2001.

[15] J. A. Encinar and J. A. Zornoza, "Broadband Design of Three-Layer Printed Reflectarrays," *IEEE Transactions on Antennas and Propagation*, vol. 51, July 2003.

[16] J. Huang, "A Ka-Band Microstrip Reflectarray with Elements Having Variable Rotation Angles," *IEEE Transactions on Antennas and Propagat*ion, vol. 46, no. 5, pp. 650-656, May 1998.

[17] A. W. Robinson, M.E. Bialkowski, and H.J. Song, "An X-Band Passive Reflect-Array Using Dual-Feed Aperture Coupled Patch Antennas," *Asia Pacific Microwave Conference*, pp. 906-909, Dec. 1999.

[18] E. Carrasco, M. Barba, and J. A. Encinar, "Aperture-Coupled Reflectarray Element with Wide Range of Phase Delay," *Electronics Letters*, vol. 42, no. 12, pp. 667–668, June 2006.

[19] J. A. Encinar and J. A. Zornoza, "Broadband Design of Three-Layer Printed Reflectarrays," *IEEE Transactions on Antennas and Propagation*, vol. 51, pp. 1662-1664, July 2003.

[20] M. E. Bialkowski, A. W. Robinson, and H. J. Song, "Design, Development, and Testing of X-Band Amplifying Reflectarryas," *IEEE Transactions on Antennas and Propagation*, pp. 1065 – 1076, Aug. 2002.

[21] M. E. Cooley, T. J. Chwalek, and P. Ramanujam, "Method for Improving Pattern Bandwidth of Shaped Beam Reflectarray," *Patent US* 6031506, (Feb. 2000).

[22] O. M. Bucci, G. Franceschetti, G. Mazzarella, G. Panariello, "Intersection Approach to Array Pattern Synthesis," *IEE Proceedings*, vol. 137, pt. H, no. 6, pp. 349-357, Dec. 1990.

[23] J. A. Encinar and J. A. Zornoza, "Three-Layer Printed Reflectarrays for Contoured Beam Space Applications," *IEEE Transactions on Antennas and Propagation*, vol. 52, no. 5, pp. 1138-1148, May 2004.

[24] M. Arrebola, J. A. Encinar, Y. Alvarez, and F. Las-Heras, "Design and Evaluation of a Three-Beam LMDS Central Station Antenna Using Reflectarrays," *MELECOM 2006*, Malaga, Spain, pp. 328-331, May 2006.

[25] R. R. Romanofsky, J. T. Bernhard, F. W. van Keuls, F. A. Miranda, G. Washington, and C. Canedy. "K-Band Phased Array Antennas Based on Ba0.60Sr0.40Tio3 Thin-Film Phase Shifters," *IEEE Transactions on Microwave Theory and Techniques*, vol. 48, pp. 2504 - 2510, Dec. 2000.

[26] A. Mössinger, R. Marin, S. Mueller, J. Freese, and R. Jakoby, "Electronically Reconfigurable Reflectarrays with Nematic Liquid Crystals," *IEE Electronics Letters*, vol. 42, pp. 899-900, Aug. 2006.

[27] R. Marin, A. Mössinger, J. Freese, and R. Jakoby, "Characterisation of 35 GHz Tunable Reflectarray Unit Cells Using Highly Anisotropic Liquid Crystal," *German Microwave Conference(GeMIC)*, Karlsruhe, Germany, 28-30 March 2006.

[28] F. Venneri, L. Boccia, G. Angiulli, G. Amendola, and G. Di Massa, "Analysis and Design of Passive and Active Microstrip Reflectarrays," *Int. Journal of RF and Microwave Computer-Aided Eng.*, vol. 13, pp. 370-377, 2003.

[29] S. V. Hum, M. Okoniewski, and R. J. Davies, "Realizing an Electronically Tunable Reflectarray Using Varactor Diode-Tuned Elements," *IEEE Microwave and Wireless Components Letters*, vol. 15, Issue 6, pp. 422-424, June 2005.

[30] D. F. Sievenpiper, J. H. Schaffner, H. J. Song, R. Y. Loo, and G. Tangonan, "Two-Dimensional Beam Steering Using an Electrically Tunable Impedance Surface," *IEEE Transactions on Antennas and Propagation,* vol. 51, Issue 10, Part 1, pp. 2713-272, Oct. 2003.

[31] J. Huang, "Analysis of a Microstrip Reflectarray Antenna for Microspacecraft Applications," *NASA TDA progress report,* pp. 153-173, Feb. 1995.

[32] R. J. Richards, E.W. Dittrich, O.B. Kesler, and J.M. Grimm, "Microstrip Phase Shifting Reflect Array Antenna," *Patent US* 6020853, (Feb. 2000).

[33] R. J. Richards, "Integrated Microelectromechanical Phase Shifting Reflect Array Antenna," *Patent US* 6195047, (Feb. 2001).

[34] H. Legay, B. Pinte, M. Charrier, A. Ziaei, E. Girard, and R. Gillard, "A Steerable Reflectarray Antenna with MEMS Controls," *IEEE International Symposium on Phased Array Systems and Technology*, pp. 494-499, 14-17 Oct. 2003.

[35] E. Girard, R. Moulinet, R. Gillard, and H. Legay, "An FDTD Optimization of a Circularly Polarized Reflectarray Unit Cell," *IEEE Antennas and Propagat. Int. Symposium*, pp. 136-139, 2002.

[36] R. Gilbert, "Dipole Tunable Reconfigurable Reflector Array," *Patent US* 2001/0050650, (Dec. 2001).

[37] H. P. Hsu and T. Y. Hsu, "Optically Controlled RF MEMS Switch Array for Configurable Broadband Reflective Antennas," *Patent US* 6417807, (Jul. 2002).

[38] G. Rebeiz, G. L. Tan, and J. S. Hayden, "RF MEMS Phase Shifters: Design and Applications," *IEEE Microwave Magazine*, pp. 72-81, June 2002.

[39] H. Legay, G. Caille, E. Girard, P. Pons, H. Aubert, E. Perret, P. Calmon, J. P. Polizzi, J. P. Ghesquiers, D. Cadoret, and R. Gillard, "MEMS Controlled

Linearly Polarised Reflect Array Elements," *12th International Symposium on Antenna Technology and Applied Electromagnetics (ANTEM)*, Montréal, 16-19 July 2006.

[40] E. Perret, N. Raveu, H. Aubert, and H. Legay, "Scale Changing Technique for MEMS-Controlled Phase Shifters," *36th EuMC*, Manchester, pp. 866-869, 10-15 September 2006.

[41] L. Marcaccioli, B. Mencagli, R. Vincenti Gatti, T. Feger, T. Purtova, H. Schumacher, and R. Sorrentino, "Beam Steering MEMS mm-Wave Reflectarrays," *MEMSWAVE 2006*, Orvieto, Italy, 27-30 June 2006.

[42] B. Mencagli, R. Vincenti Gatti, L. Marcaccioli, and R. Sorrentino, "Design of Large mm-Wave Beam-Scanning Reflectarrays," *35th EuMC*, Paris, 3-7 Oct. 2005.

[43] A. W. Robinson, M. E. Bialkowski, and H. J. Song, "An 137-Element Active Reflect-Array with Dual-Feed Microstrip Patch Elements," *Microwave and Optical Technology Letters*, vol. 26, no. 3, pp. 147-151, Aug. 2000.

[44] D. M. Pozar and D. H. Schaubert, "Scan Blindness in Infinite Phased Arrays of Printed Dipoles," *IEEE Transactions on Antennas and Propagation*, vol. AP-32, pp. 602-620, June 1984.

[45] D. M. Pozar, "Microstrip Antenna Aperture-Coupled to a Microstripline," *Electronics Letters*, vol. 21, no. 2, pp. 49-50, Jan. 1985.

[46] D. Jaisson, "Transmission Line Model for the Input Impedance of a Slot-Coupled Rectangular Patch Antenna," *IEE Proceedings on Microwaves, Antennas and Propagation*, vol. 153, pp. 461-468, Oct. 2006.

[47] M. Himdi, J. P. Daniel, and C. Terret, "Analysis of Aperture-Coupled Microstrip Antenna Using Cavity Method," *Electronics Letters*, vol. 25, no. 6, pp. 391–392, March 1989.

[48] P. L. Sullivan and D. H. Schaubert, "Analysis of an Aperture Coupled Microstrip Antenna," *IEEE Transactions on Antennas and Propagation*, vol. AP-34, pp. 977-984, Aug. 1986.

[49] F. Alimenti, F. Tiezzi, R. Sorrentino, S. Lindenmeier, L. Pierantoni, and P. Russer, "Accurate Analysis and Modeling of Slot Coupled Patch Antennas by the TLM-IE and the FDTD Methods," *28th EuMC*, vol. 1, pp. 30-35, Oct. 1998.

[50] M. Himdi, J. P. Daniel, and C. Terret, "Transmission Line Analysis of Aperture-Coupled Microstrip Antenna," *Electronics Letters*, vol. 25, no. 18, pp. 1299-1230, Aug. 1989.

[51] J. R. James and P. S. Hall, "Handbook of Microstrip Antennas," *Peter Peregrinus*, 1989.

[52] S. B. Cohn, "Slot Line on a Dielectric Substrate," *IEEE Transactions on Microwave Theory and Techniques*, vol. 17, pp. 768-778, Oct. 1969.

[53] M. Himdi and J. P. Terret, "Characteristics of Sandwich Slot Lines In Front of a Parallel Metallic Strip," *Electronics Letters*, vol. 27, pp. 455-457, 28 Feb. 1991.

[54] D. M. Pozar, "A Review of Aperture Coupled Microstrip Antennas: History, Operation, Development, and Applications," *Internal Report of Electrical and Computer Eng., University of Massachusetts Amherst*, 1996.

[55] R. E. Munson, H. Haddad, and J. Hanlen, "Microstrip Reflectarray Antenna for Satellite Communication and RCS Enhancement or Reduction," *U.S. Patent* 4684952, (Aug. 1987).

[56] J. Hnang, "Microstrip Reflectarray," *IEEE Int. Symp. on Antennas and Propagation*, Ontario, Canada, pp. 612-615, June 1991.

[57] D. C. Chang and M. C. Huang, "Microstrip Reflectarray Antenna with Offset Feed," *Electronics Letters*, vol. 28, pp. 1489-1491, July 1992.

[58] D. M. Pozar and T. A. Metzler, "Analysis of a Reflectarray Antenna Using Microstrip Patches of Variable Size," *Electronics Letters*, vol. 29, pp. 657-658, 1993.

[59] S. D. Targonski and D. M. Pozar, "Analysis and Design of a Microstrip Reflectarray Using Patches of Variable Size," *Int. Symp. on Antennas and Propagation*, Seattle, WA, pp. 1820-1823, June 1994.

[60] M. Bozzi, S. Germani, and L. Perregrini, “Performance Comparison of Different Element Shapes Used in Printed Reflectarrays,” *IEEE Antennas Wireless Propagation Letters*, vol. 2, pp. 219-222, 2003.

[61] M. R. Chaharmir, J. Shaker, M. Cuhaci, and A. Sebak, “Reflectarray with Variable Slots on Ground Plane,” *IEE Proceedings on Microwaves Antennas and Propagion*, vol. 150, no 6, pp. 436-439, Dec. 2003.

[62] N. Lenin and Patnam H. Rao, “Evaluation of the Reflected Phase of a Patch Using Waveguide Simulator for Reflectarray Design,” *Microwave and Optical Technology Letters*, vol. 45, no. 6, pp. 528-531, 2005.

[63] Discussion with Julien Perruisseau-Carrier, *Laboratory of electromagnetics and acoustics, Ecole Polytechnique Fédérale de Lausanne (EPFL).*

[64] E. Carrasco, M. Barba, and J. A. Encinar, “Reflectarray Element Based on Aperture-Coupled Patches with Slots and Lines of Variable Length,” *IEEE Transactions on Antennas and Propagation*, vol. 55, pp. 820-825, March 2007.

[65] P. Farinelli, T. Vähä-Heikkilä, J. Säily, R. Sorrentino, and J. Tuovinen, “A Novel Method for Millimeter-Wave On-Wafer Characterization of Reflect Patch Antennas,” *IEEE Antennas and Wireless Propagation Letters*, vol. 5, nr. 1, pp. 556-558, 2006.

APPENDIX A

MEASUREMENT TECHNIQUES

The measurement set up shown in Figure A1 is used to measure the whole reflectarray. In this configuration, the reflectarray is placed on the chuck with the help of a support material which is chosen as a foam for not to be affected from its electromagnetic properties. On the circular chuck, there is also feed horn antenna used to illuminate the reflectarray surface and absorber for avoiding the scattering from the coaxial cable. The reflectarray surface is placed at z=0 plane and the circular chuck can be rotated at the center (y-axis). Using the reciprocity principle, the reflectarray is illuminated by a pick-up horn and the reflections are measured by the feed horn while the chuck is rotating. By this method the reflectarray pattern is obtained.

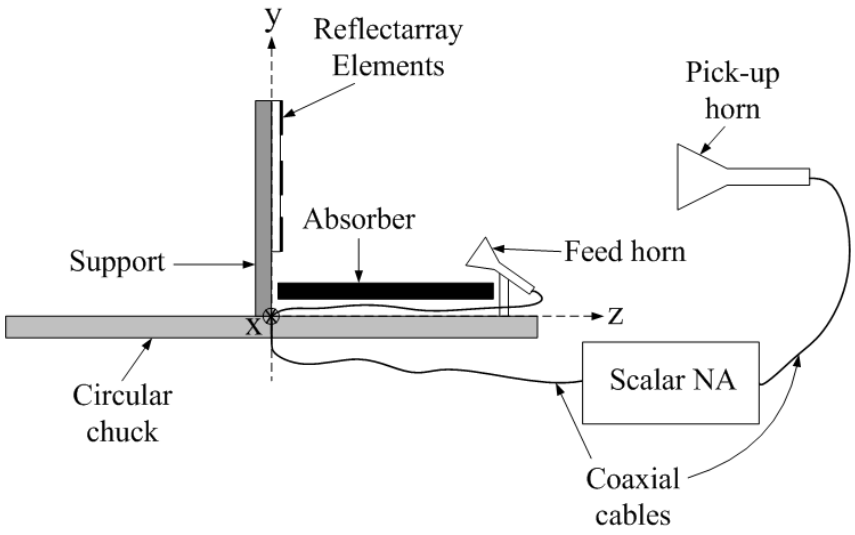

Figure A1: The direct measurement of the reflectarray.

In order to obtain the reflection phase characteristics of the unit cell, the wave guide simulator is proposed by Lenin et al. as shown in Figure A2 [62]. In this method the unit cell structures having bilateral symmetry is used as discussed in Section 3.1.1. The design and measurements are carried out at 10GHz in [62]. This method restricts the unit cell dimension with the aperture of the available waveguide.

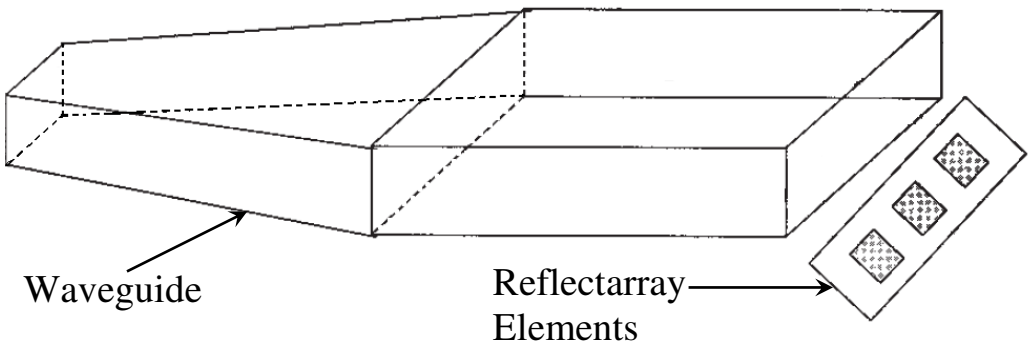

Figure A2: The wave guide method used to measure the single element [62].

The other method suggested by Paulo et al. [65] is to measure the reflectarray unit cells on the wafer. The measurements in [65] are carried out at 57.2 GHz. In this case, it is difficult to construct the small horn antenna for the measurement.

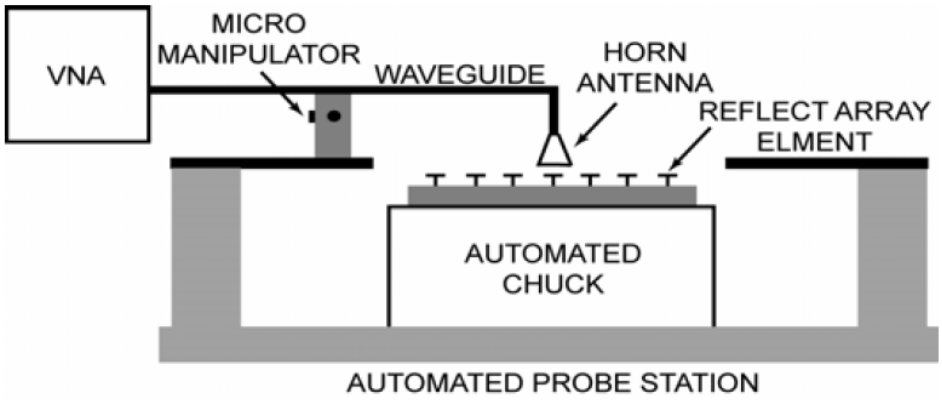

Figure A3: The measurement set up constructed for the single element measurement [65].

APPENDIX B

FINAL PHASE SHIFTER LENGTHS

Figure B1 shows the matrix representation of the reconfigurable reflectarray where the squares represent the ACMPA elements. The numbers in the squares are costructed by writing first the row number and then column number of the ACMPA. The phase shifter dimensions for each ACMPA are given in Table B1 where the corresponding phase shifter structure can be found in Figure B2.

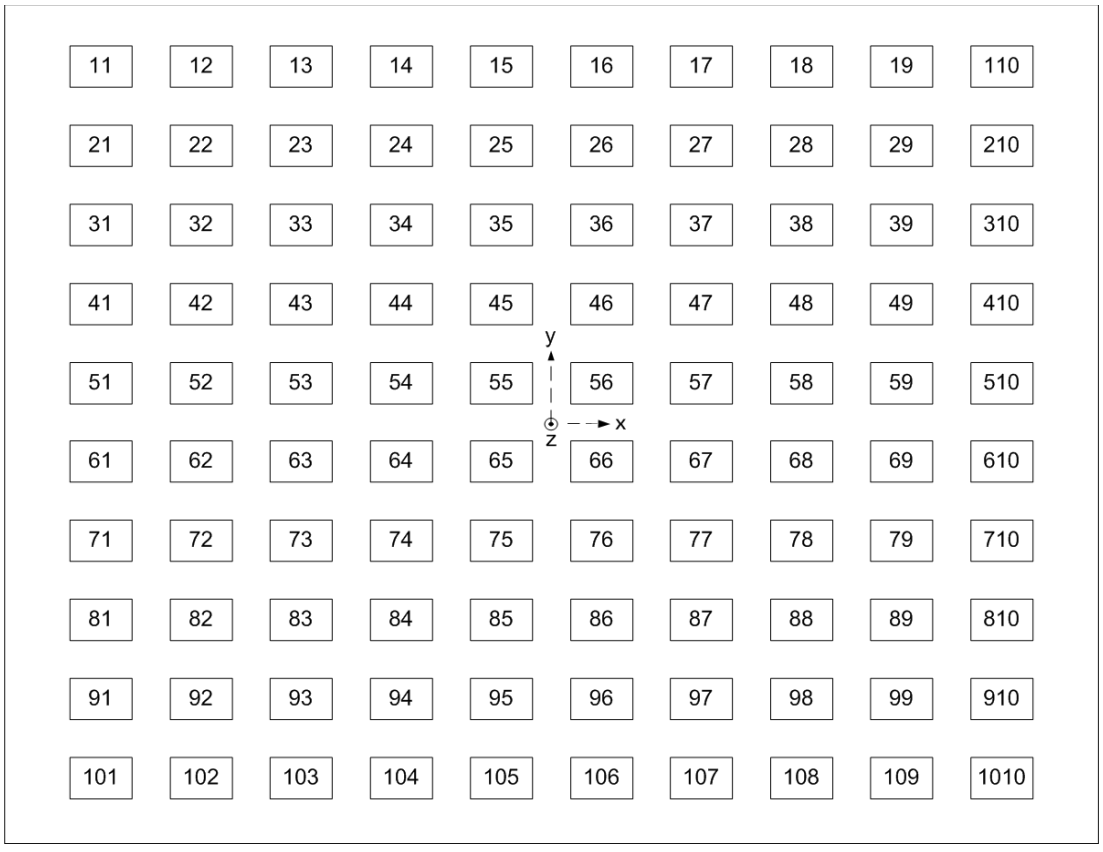

Figure B1: The symbolic matrix representation of the reflectarray.

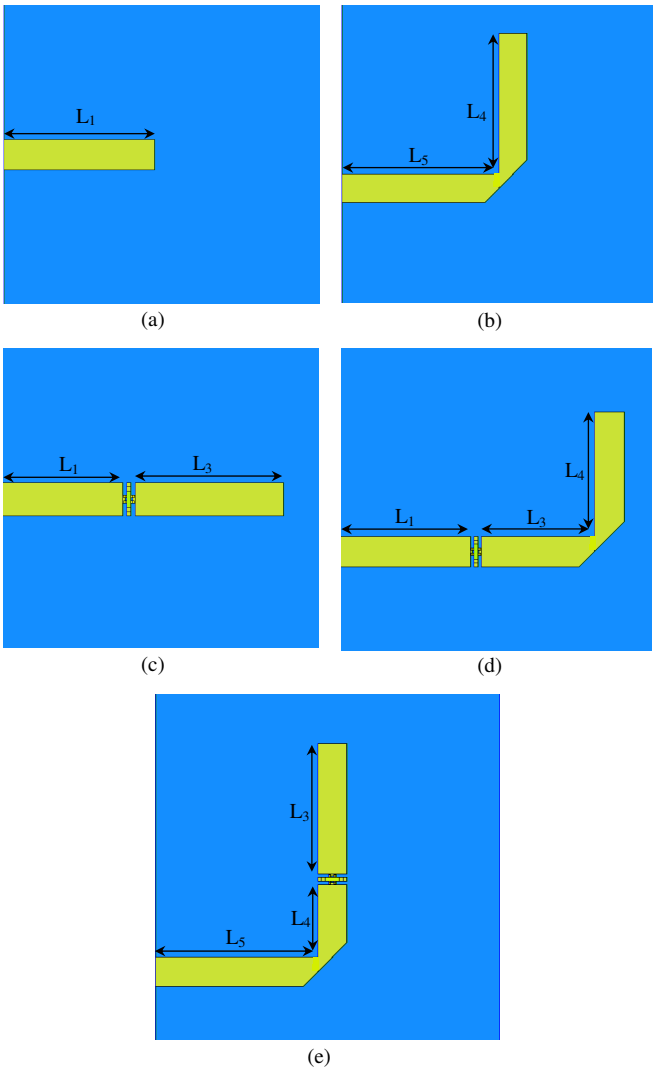

Figure B2: The possible phase shifter parts of the elements of the reconfigurable reflectarray.

Table B1: The distribution of the phase shifter dimensions shown in Figure B1 in the elements of the reflectarray (NA: Not Applicable).

Element of the array	L_1 (μm)	L_3 (μm)	L_4 (μm)	L_5 (μm)
11	754	NA	NA	NA
21	1510	NA	NA	NA
31	2235	NA	NA	NA
41	NA	NA	612	2230
51	584	NA	NA	NA
61	1220	NA	NA	NA
71	1825	NA	NA	NA
81	2410	NA	NA	NA
91	NA	NA	612	2230
101	410	NA	NA	NA
12	810	822	NA	NA
22	1565	842	NA	NA
32	2316	200	520	NA
42	NA	810	670	2230
52	650	822	NA	NA
62	1286	842	NA	NA
72	1902	200	530	NA
82	2490	200	520	NA
92	NA	802	680	2230
102	500	818	NA	NA
13	866	1214	562	NA
23	1643	437	1279	NA
33	NA	1775	200	2120
43	NA	1865	726	2230
53	717	1873	NA	NA
63	1359	721	1019	NA
73	1985	200	1500	NA
83	NA	1796	256	2230
93	NA	1866	750	2230
103	569	1873	NA	NA
14	963	1117	1750	NA
24	1700	380	2520	NA
34	NA	2960	200	2182
44	140	1940	935	NA

54	810	1270	1605	NA
64	1442	638	2252	NA
74	2040	200	2717	NA
84	NA	2972	330	2230
94	150	1930	960	NA
104	665	1415	1455	NA
15	1037	725	NA	NA
25	1803	278	362	NA
35	NA	655	232	2230
45	205	733	NA	NA
55	884	720	NA	NA
65	1529	735	NA	NA
75	2152	200	420	NA
85	NA	675	406	2230
95	230	723	NA	NA
105	739	723	NA	NA
16	990	1090	565	NA
26	1762	318	1271	NA
36	NA	1661	204	2230
46	146	1760	NA	NA
56	843	1237	420	NA
66	1486	594	1010	NA
76	2120	200	1367	NA
86	NA	1694	362	2230
96	165	1760	NA	NA
106	700	1745	NA	NA
17	824	1256	1748	NA
27	1577	503	2515	NA
37	2310	200	2843	NA
47	NA	3100	700	2230
57	671	1409	1595	NA
67	1307	773	2243	NA
77	1916	200	2825	NA
87	NA	3085	210	2230
97	NA	3125	710	2230
107	528	1552	1450	NA
18	932	620	NA	NA
28	1697	620	NA	NA
38	NA	560	200	2170

48	NA	604	780	2230
58	770	620	NA	NA
68	1410	635	NA	NA
78	2023	635	NA	NA
88	NA	570	300	2230
98	NA	605	810	2230
108	626	620	NA	NA
19	775	1632	NA	NA
29	1535	545	950	NA
39	2286	200	1250	NA
49	NA	1590	640	2230
59	623	1605	NA	NA
69	1254	826	690	NA
79	1880	200	1250	NA
89	2465	200	1240	NA
99	NA	1605	648	2230
109	470	1600	NA	NA
110	365	1715	1400	NA
210	1129	951	2166	NA
310	1850	230	2910	NA
410	NA	3196	260	2230
510	196	1884	1240	NA
610	840	1240	1880	NA
710	1440	640	2493	NA
810	2007	200	2952	NA
910	NA	3192	264	2230
1010	NA	3233	730	2230